Frozen-soil hydrological modeling for a mountainous catchment at northeast of the Qinghai-Tibet Plateau

Hongkai Gao 1, 2, 3*, Chuntan Han 34, Rensheng Chen 34, Zijing Feng 2, Kang Wang 1,2, Fabrizio Fenicia 45, Hubert Savenije 56

1 Key Laboratory of Geographic Information Science (Ministry of Education of China), East China Normal University, Shanghai, China

2 School of Geographical Sciences, East China Normal University, Shanghai, China

3 State Key Laboratory of Tibetan Plateau Earth System and Resources Environment (TPESRE), Institute of Tibetan Plateau Research, Chinese Academy of Sciences, Beijing, China.

3 4 Qilian Alpine Ecology and Hydrology Research Station, Key Lab. of Ecohydrology of Inland River Basin, Northwest Institute of Eco-Environment and Resources, Chinese Academy of Sciences, Lanzhou 730000, China

4 5 Eawag, Swiss Federal Institute of Aquatic Science and Technology, Dubendorf, Switzerland

5 6 Delft University of Technology, Delft, the Netherlands

*Corresponding to: Hongkai Gao (hkgao@geo.ecnu.edu.cn; gaohongkai2005@126.com)

Abstract:

Increased attention directed at frozen-soil hydrology has been prompted by climate change. In spite of an increasing number of field measurements and modeling studies, the impact of frozen-soil on hydrological processes at the catchment scale is still unclear. However, frozen-soil hydrology models have mostly been developed based on a "bottom-up" approach, i.e. by aggregating prior knowledge at pixel scale, which is an approach notoriously suffering from equifinality and data scarcity. Therefore, in this study, we explore the impact of frozen-soil at catchment-scale, following a "top-down" approach, implying: expert-driven data analysis → qualitative perceptual model → quantitative conceptual model → testing of model realism. The complex mountainous Hulu catchment, northeast of the Qinghai-Tibet Plateau (QTP), was selected as the study site. Firstly, we diagnosed the impact of frozen-soil on catchment hydrology, based on multi-source field observations, model discrepancy, and our expert knowledge. Two new typical hydrograph properties were identified: the low runoff in the early thawing season (LRET) and the discontinuous baseflow

recession (DBR). Secondly, we developed a perceptual frozen-soil hydrological model, to explain the LRET and DBR properties. Thirdly, based on the perceptual model and a landscape-based modeling framework (FLEX-Topo), a semi-distributed conceptual frozen-soil hydrological model (FLEX-Topo-FS) was developed. The results demonstrate that the FLEX-Topo-FS model can represent the effect of soil freeze/thaw processes on hydrologic connectivity and groundwater discharge and significantly improve hydrograph simulation, including the LRET and DBR events. Furthermore, its realism was confirmed by alternative multi-source and multi-scale observations, particularly the freezing and thawing front in the soil, the lower limit of permafrost, and the trends in groundwater level variation. To the best of our knowledge, this study is the first report of LRET and DBR processes in a mountainous frozen-soil catchment. The FLEX-Topo-FS model is a novel conceptual frozen-soil hydrological model, which represents these complex processes and has potential for wider use in the vast QTP and other cold mountainous regions.

1 Introduction

1.1 Frozen-soil hydrology: one of twenty-three unsolved problems

The Qinghai-Tibet Plateau (QTP) is largely covered by frozen soil and is characterized by a fragile cold and arid ecosystem (Immerzeel et al., 2010; Ding et al., 2020). As this region serves as the "water tower" for nearly 1.4 billion people, understanding the frozen soil hydrology is important for regional and downstream water resources management and ecosystem conservation. Frozen soil prevents vertical water flow which often leads to saturated soil conditions in continuous permafrost, while confining subsurface flow through perennially unfrozen zones in discontinuous permafrost (Walvoord and Kurylyk, 2016). As an aquiclude layer, frozen soil substantially controls surface runoff and its hydraulic connection with groundwater. The freeze–thaw cycle in the active layer significantly impacts soil water movement direction, velocity, storage capacity, and hydraulic conductivity (Bui et al., 2020; Gao et al., 2021).

Frozen-soil hydrology attracts increasing attention, as the cold regions, e.g. QTP and Arctic, are undergoing rapid changes (Song et al., 2020; Tananaev et al., 2020). Frozen-soil thawing also poses great threats to the release of frozen carbon in both high altitude and latitude regions, which is likely to create substantial impacts on the climate system (Wang et al., 2020). Attention is also growing for the impact of frozen-soil hydrology on nutrient transport and organic matter, and frozen soil–climate feedback (Tananaev et al., 2020). Hence, there are strong motivations to better understand frozen-soil hydrological processes (Bring et al., 2016).

Frozen-soil degradation and its impact on hydrology is one of the research frontiers for the hydrologic community (Blöschl et al., 2019; Zhao et al., 2020; Ding et al., 2020). "How will cold region runoff and groundwater change in a warmer climate?" was identified by the

73 International Association of Hydrological Sciences (IAHS), as one of the 23 major unsolved
74 scientific problems (Blöschl et al., 2019), which requires stronger harmonization of
75 community efforts.

1.2 The frontier of frozen-soil hydrology

77 Knowledge on frozen-soil hydrology was acquired through detailed investigations at
78 isolated locations over various time spans by hydrologists and geocryologists (Woo et al.,
79 2012; Gao et al., 2021). At the core scale, there are many measurements of soil profiles,
80 including but not limited to soil temperature (Kurylyk et al., 2016; Han et al., 2018), soil
81 moisture (Dobinski, 2011; Chang et al., 2015), groundwater fluctuation (Ma et al., 2017;
82 Chiasson-Poirier et al., 2020), and active layer seasonal freeze-thaw processes (Wang et al.,
83 2016; Farquharson et al., 2019). At the plot/hillslope scale, land surface energy and water
84 fluxes are measured by eddy covariance, large aperture scintillometer (LAS), lysimeter, and
85 multi-layers meteorological measurements. Geophysical detection technology allows us to
86 measure various subsurface permafrost features. At the basin scale, except for traditional
87 water level and runoff gauging, water sampling and the measurements of isotopes and
88 chemistry components provide important complementary data to understand catchment
89 scale hydrological processes (Streletskiy et al., 2015; Ma et al., 2017; Yang et al., 2019).
90 Remote sensing technology, including optical, near- and thermal-infrared, passive and
91 active microwave remote sensing, has been used to identify surface landscape features (e.g.
92 vegetation and snow cover) and directly or indirectly retrieve subsurface variables (e.g.
93 near-surface soil freeze/thaw and permafrost state) in frozen-soil regions (Nitze et al., 2018;
94 Jiang et al., 2020).

95 Besides measurement, modeling provides another indispensable dimension to understand
96 frozen-soil hydrology in an integrated way, and make predictions in climate change. There
97 has been a revival in the development of frozen-soil hydrological models simulating
98 coupled heat and water transfer. Such physically-based models typically calculate seasonal
99 freeze–thaw through solving heat transfer equations. Such equations are either solved
100 analytically or numerically (Walvoord and Kurylyk, 2016). The Stefan equation is a typical
101 example of the analytical approach, which calculates the depth from the ground surface to
102 the thawing (freezing) horizon by the integral of ground surface temperature and soil
103 features. The Stefan equation is widely used to estimate active layer thickness (Zhang et al.,
104 2005; Xie and Gough, 2013), and is incorporated into some hydrological models (Wang L,
105 2010; Fabre et al. 2017). The numerical solution schemes (e.g., finite difference, finite
106 element, or finite volume) to model ground freezing and thawing, is typically applied to
107 one-dimensional infiltration into frozen soils, and is included in models such as SHAW (Liu
108 et al., 2013), CoupModel (Zhou et al., 2013), the distributed water-heat coupled (DWHC)
109 model (Chen et al. 2018), the distributed ecohydrological model (GBEHM) (Wang Y. 2018),
110 and the three-dimensional SUTRA model (Evans et al. 2018). Andresen et al (2020)
111 compared 8 permafrost models on soil moisture and hydrology projection across the major
112 Arctic river basins, and found that the projection varied strongly in magnitude and spatial
113 pattern. Except for hydrological models, many land surface models explicitly consider the

114 freeze-thaw process, in order to improve land surface water and energy budget estimation
115 and weather forecasting accuracy in frozen-soil areas. Such models include VIC (Cuo et al.,
116 2015), JULES (Chadburn et al., 2015), CLM (Niu et al., 2006; Oleson et al., 2013; Gao et al.,
117 2019), CoLM (Xiao et al., 2013), Noah-MP (Li et al., 2020), ORCHIDEE (Gouttevin et al.,
118 2012). Comprehensive reviews on frozen-soil hydrological models can be found in
119 Walwoord and Kurylyk (2016), Jiang et al. (2020), and Gao et al. (2021).

1.3 The challenge of frozen-soil hydrological modeling

121 Although numerous frozen-soil hydrological models were developed, most models have
122 strong prior assumptions on the impacts of frozen-soil on hydrological behavior (Walvoord
123 and Kurylyk, 2016; Gao et al., 2021). Such models follow a "bottom-up" modeling approach,
124 which presents an "upward" or "reductionist" philosophy, based on the aggregation of
125 small-scale processes and *a priori* perceptions (Jarvis, 1993; Sivapalan et al., 2003). However,
126 most of the "upward" process understanding has been obtained from in-situ observation
127 and in-situ modeling, which have limited spatial and invariably limited temporal coverage
128 (Brutsaert, and Hiyama, 2012). It is worthwhile to note that frozen-soil has tremendous
129 spatial-temporal heterogeneities, which are strongly influenced by many intertwined factors,
130 including but not limited to climate, topography, geology, soil texture, snow cover, and
131 vegetation. Upscaling could average out some variables, and turn other variables visible and
132 even become dominant processes (Fenicia and McDonnell, 2022). Unfortunately, translating
133 spot/hillslope scale frozen-soil process to its influence on catchment scale hydrology,
134 guided by carefully expert analysis, and constrained by multi-source measurements, is still
135 largely unexplored.

136 The effects of the soil freeze/thaw process on hydrology at catchment scale is still
137 inconclusive. In the headwaters of the Yellow River, some modeling studies concluded that
138 permafrost has significant impact on streamflow (Sun et al., 2020). But in Sweden and the
139 northeast of the United States, other studies found frozen soil have negligible impact on
140 streamflow (Shanley and Chalmers, 1999; Lindstrom et al., 2002). Some studies found that
141 the impact of frozen soil on streamflow is concentrated in certain periods. For example,
142 Osuch et al. (2019) found permafrost to impact on groundwater recession and storage
143 capacity of the active layer in Svalbard Island; Nyberg et al. (2001) found that in the Vindeln
144 Research Forest in northern Sweden permafrost impacted streamflow only in springs.
145 Hence, we argue that the impact of local scale freeze-thaw process on runoff should be
146 regarded as a hypothesis to be verified or rejected.

147 The unexplored frozen-soil hydrology is especially true for mountainous Asia, due to the
148 lack of long-term observations as a result of the difficulty of access and high cost of
149 operation. The cold region of the QTP is characterized by relatively thin and warm frozen-
150 soil with low ice content, due to the unique environmental conditions, arid climate, high
151 elevation and steep geothermal gradient (Cao et al., 2019; Zhao et al., 2020; Jiang et al.,
152 2020). Snow cover is thinner, and vegetation cover is poorer than in Arctic regions. These
153 features limit the insulation effect on freeze-thaw processes, resulting in a much larger
154 active layer depth (Pan et al., 2016). Topographical features, including elevation and aspect,

155 are major factors affecting permafrost distribution. The complex mountainous terrain, as a
156 result of recent tectonic movement, leads to large spatial heterogeneity in the energy and
157 water balance, and underexplored frozen-soil hydrology on the QTP (Gao et al., 2021).

1.4 Aims and scope

159 In this study, we utilized a "top-down" approach (Sivapalan et al., 2003), to understand the
160 effect of frozen-soil on hydrology in the Hulu catchment on the northeastern edge of the
161 QTP. The aims of this study are as below:

162 1) Diagnosing the impacts of frozen-soil on hydrology in the mountainous Hulu
163   catchment, with multi-source, multi-scale data and model discrepancy;

164 2) Developing a quantitative conceptual frozen-soil hydrological model, based on expert-
165   driven interpretation in the form of perceptual model for the Hulu catchment;

166 3) Testing the realism of the conceptual frozen-soil hydrological model, with multi-source
167   and multi-scale observations.

168 In this paper, we firstly introduced the study site and data in Section 2; an expert-driven
169 perceptual frozen-soil hydrology model was proposed in Section 3; a semi-distributed
170 conceptual frozen-soil hydrological model, FLEX-Topo-FS, was developed in Section 4; the
171 realism of the FLEX-Topo-FS model was tested in Section 5; in Section 6 and 7, last but not
172 least, we made discussions and draw the conclusions.

2 Study site and data

174 The Hulu catchment (38°12′–38°17′ N, 99°50′–99°54′E) is located in the upper reaches of
175 the Heihe River basin, the northeast edge of the QTP in northwest China (Figure 1). The
176 elevation ranges from 2960 to 4820 m a.s.l., gradually increasing from north to south (Figure
177 1) (Chen et al., 2014; Han et al., 2018). Most precipitation occurs in the summer monsoon
178 time, and snowfall in winter is limited (Han et al., 2018; Jiang et al., 2020). There is a runoff
179 gauging station at the outlet, controlling an area of 23.1 km^2. Two minor tributaries are
180 sourced from glaciers (east) and moraine–talus (west) zones, which merge at the catchment
181 outlet. The Hulu catchment has rugged terrain and very little human disturbance. We
182 identified four main landscape types, i.e. glaciers (5.6%), alpine desert (53.5%), vegetation
183 hillslope (37.5%), and riparian zone (3.4%) (Figure 2).

184 The Hulu catchment mostly extends on seasonal frozen-soil and permafrost (Zou et al.,
185 2014; Ma et al., 2021). Field survey in the upper Heihe revealed that the lower limit of
186 permafrost was 3650m~3700m (Wang et al., 2013), above that elevation is permafrost, and
187 below is seasonal frozen-soil. In the Hulu catchment, the lower limit of permafrost is around
188 3650m (Figure 1). Permafrost covers 64% of the catchment area, and the seasonal frozen-
189 soil covers 36%. There is a strong co-existence between soil freeze-thaw feature and
190 landscapes (Figure 1). Permafrost and moraine/talus with poor vegetation cover co-exist in
191 higher elevation, with large heat conductivity and less heat insulation in winter, resulting

192 deep frozen depth. The seasonal frozen soil in relative lower elevation has better vegetation
193 cover, with better heat insulation and less heat conductivity in winter, resulting in shallower
194 frozen depth.

195 The elevation of the hydrometeorological gauging station is 2980m. We collected daily
196 runoff, daily average 2m air temperature, and daily precipitation from January 1st 2011 to
197 December 31st 2014. There was a flood event in 2013, which damaged the water level
198 sensor, resulted in a runoff data gap from June 17th to July 10th in 2013. Soil moisture was
199 measured in 20cm, 40cm, 80cm, 120cm, 180cm, 240cm, and 300cm depths from October 1st
200 2011 to December 31st 2013, with a data gap between August 3rd 2012 and October 2nd
201 2012. In the same soil moisture site, we also observed the soil freeze/thaw depth from 2011
202 to 2014. Groundwater depth was measured at WW01 site by four wells, with depth of 5m,
203 10m, 15m, and 25m respectively (Pan et al., 2021). The observation period was from 2016 to
204 2019, not overlaid with other hydrometeorological variables. Hence, we merely used the
205 groundwater level to qualitatively constrain and test our perceptual model.

3 An expert-driven perceptual frozen-soil hydrology model

based on field observations

208 Perceptual model is increasingly recognized as the central importance in hydrological
209 model development (Fenicia and McDonnell, 2022). Although perceptual model is a
210 qualitative representation of hydrological system, it bridges the gap between
211 experimentalists and modelers, and hold the base for quantitative conceptual model. In this
212 study, we developed a perceptual frozen-soil hydrology model for the Hulu catchment,
213 based on field measurements and our expertise.

3.1 Observation1: Low runoff in the early thawing season (LRET)

215 Precipitation-runoff time series analysis is a tradition and powerful tool to understand
216 catchment hydrology. When we plot Hulu catchment's precipitation and runoff data
217 together, we observed an interesting phenomenon, i.e. low runoff in the early thawing
218 season (LRET) (Figure 3). For example, on June 5-9, 2013, there was a 45.7mm rainfall event,
219 with air temperature ranging from 3.0℃ to 11.9℃, but with only 0.68mm in total runoff
220 generation. Ma et al., (2021) also showed that in the warm middle June 2015 in Hulu
221 catchment, there was a large rainfall event (over 30mm/d), but no runoff response was
222 observed. Moreover, this LRET phenomenon repeatedly happens every year, which allows
223 us to exclude the possibility of measurement errors.

224 To further investigate the LRET phenomenon, we plot the time series of observed daily
225 precipitation, temperature, runoff, freeze/thaw front depth, and soil moisture profile (20cm,
226 120cm, and 240cm) together (Figure 3). Soil moisture data showed that top soil was dry at
227 the beginning of thawing season. Gradually, soil was thawing from both topsoil and

228 downwards (Figure 3), and simultaneously the soil moisture was increased also downwards.
229 Although the topsoil was thawed, there was still frozen-soil underneath (Figure 3). The
230 water above the frozen-soil layer was even saturated with ponding but no percolation and
231 runoff generation. Moreover, the groundwater level further declined (Figure 11). This
232 illustrated that, during this period, the soil and groundwater system were disconnected, very
233 likely because the frozen soil blocked the percolation. As revealed by isotope data in the
234 Hulu catchment, groundwater contributed the dominant streamflow, i.e. 95% during the
235 frozen period (Ma et al., 2021). Thus, during this process, there was almost no runoff
236 generation, and the only contribution to streamflow during this period was the discharge
237 from groundwater system as baseflow. Our field work experience also verified that in the
238 early thawing season, vehicles were easy to be trapped in mires, because the surface soil
239 was muddy, saturated even over-saturated with ponding. When frozen-soil was completely
240 thawed in summer, trafficability became much better.

241 When completely thawed, the bidirectional thaw fronts meet, the soil moisture in the
242 bottom of frozen soil (around 2.4m in this study site, Figure 3) was increased sharply, and
243 then decreased, with a short period pulse. We also noted that the observation sites of
244 freeze/thaw front depth and soil moisture were both near the outlet of the Hulu catchment
245 in lower elevation (Figure 1). This means once the frozen soil in lower elevation was thawed,
246 soil and groundwater systems were reconnected. Hydrological processes, including
247 groundwater percolation and runoff generation, became the same as free of frozen-soil
248 normal circumstances.

249 **Learning from paired catchments**

250 The LRET phenomenon was widely documented in other cold regions (Figure 4), including
251 but not limited to the headwater of Yellow River (Yang et al., 2019), and a small headwater
252 catchment at Cape Bounty Arctic Watershed Observatory, Melville Island, NU in Canada
253 (Lafrenière and Lamoureux, 2019). For example, at the headwater of Yellow River, on July 8-
254 9 2014, there was a 21.9mm rainfall event with temperature of 6.5℃, but little 1.5m^3/s
255 runoff; and on July 21-23 2014, there was a 27.4mm rainfall event with temperature of
256 7.2℃, but only 5.1m^3/s runoff. Lafrenière and Lamoureux (2019) found that the undisturbed
257 frozen soil at Cape Bounty Arctic Watershed Observatory had little runoff generation in the
258 early thawing season. But after the frozen-soil was disturbed, the runoff response to rainfall
259 event was much larger. Hence this paired catchment study illustrated that frozen soil played
260 a key role causing the LRET phenomenon.

261 ## 3.2 Observation2: Discontinuous baseflow recession (DBR)

262 Baseflow recession provides an important source of information to infer groundwater
263 characteristic, including its storage properties, subsurface hydraulics, and concentration
264 times (Brutsaert and Sugita, 2008; Fenicia et al., 2006), which is especially true for basins with
265 frozen-soil (Ye et al., 2009; Song et al., 2020).

266 Baseflow analysis is based on the water balance equation (Equation 1), and linear reservoir
267 assumption (Equation 2). It should be noted that Equation 1 assumes no additional inflows

268 (recharge or thawing) or outflow (capillary rise or freezing). If a reservoir is linear, this
269 implies that the reservoir discharge (Q) has a linear relationship with its storage (S). K_s (days)
270 is time-constant controlling the speed of recession in the linear reservoir. With a larger K_s
271 value, the reservoir empties slower, and vice-versa. Combining Equation 1 and 2, we can
272 derive equation 3, illustrating how discharge depends on time (t), proportional to the initial
273 discharge (Q_0).

274 $$\frac{dS}{dt} = -Q \quad (1)$$

275 $$Q = S/K_s \quad (2)$$

276 $$Q = Q_0 \cdot e^{-t/Ks} \quad (3)$$

Baseflow recession analysis results

278 In Figure 5, we plot the groundwater recession on semi-logarithmic scale. In the beginning
279 of freezing season, baseflow presented a clear linear recession, and was able to be fitted by
280 setting the recession coefficient (K_s) as 80 days. However, interestingly, simultaneously with
281 the LRET phenomenon, we observed a clear discontinuous baseflow recession in the Hulu
282 catchment (Figure 5). The baseflow bended down, and K_s became 60 days in the end of
283 recession periods. This DBR phenomenon informed us that the groundwater system was
284 disturbed. We also noted the spikes during the thawing in Fig. 5, which means groundwater
285 was suddenly released. To our best knowledge, these discontinuous baseflow recession
286 (DBR) phenomenon is a new observation for mountainous frozen-soil hydrology.

287 We also plot the variation of groundwater depth of 4 wells at WW01 site from 2016 to 2019
288 (Figure 1, 11). The wells of 5m, 10m, and 15m only had liquid water in thawing seasons, and
289 gradually went dry in recession periods. The water level of the 25m well was decreasing in
290 the entire frozen seasons, but in a discontinuous way. From the observed groundwater
291 depth, the groundwater level decreases faster at beginning. And after the groundwater level
292 dropped below around 17m, the decrease of groundwater level became slower. The turning
293 point from K_s=80d to K_s =60d occurred simultaneously while the groundwater level went
294 down to 17m (Figure 5, 11). The bending down discontinuous baseflow recession and
295 slower decrease of groundwater level indicated that there was a disturbance reduced the
296 groundwater discharge and lead to a slower decrease of groundwater level.

Learning from paired catchments

298 Frozen-soil process is able to disturb the groundwater system, by freezing the liquid
299 groundwater to reduce groundwater storage, and leading to the DBR. But the DBR could
300 also be caused by many other reasons, for instance soil evaporation, root tapping, capillary
301 rise, impermeable layer, and heterogenous hydraulic conductivities in different landscapes
302 (riparian area and hillslope). Since the DBR phenomenon started from the middle of freezing
303 period, and lasted until the end of frozen season, in which time the evaporation, root
304 tapping, and capillary rise were very inactive even totally stopped, which allows us to
305 exclude these impacts. The impermeable layer and heterogenous hydraulic conductivities
306 are both able to result in discontinuous recession in small scale.

307 To further understand the DBR phenomenon, we collected larger scale runoff data in this
308 region, including the Zhamashike (5526 km^2) and Qilian (2924 km^2), which are also the sub-
309 basins of the upper Heihe. The permafrost and seasonal frozen-soil map of the upper Heihe
310 River basin shows that: the Zhamashike sub-basin has 74% permafrost and 26% seasonal
311 frozen soil, which is similar to the Hulu catchment; while the Qilian sub-basin has much less
312 permafrost area (38%), and is mostly covered by seasonal frozen-soil (62%) (Figure 1).

313 Interestingly, when plotting the hydrographs of these two sub-basins on logarithmic scale,
314 we can clearly see that in the permafrost dominated Zhamashike sub-basin discontinuous
315 recessions occurred, with K_s=60d in the early and K_s = 20d in in the end of the recession
316 period. This DBR phenomenon is the same as we found in the Hulu catchment, although the
317 Zhamashike and Hulu catchment have quite different scales (5526 km^2 versus 23.1 km^2)
318 (Chen et al. 2018, Gao et al., 2014). Discontinuous baseflow recession happened almost
319 every year at the Zhamashike station, and we only highlight the hydrograph in 1974 to
320 demonstrate this phenomenon in Figure 6. On the other hand, of similar size as the
321 Zhamashike, the Qilian sub-basin (2924 km^2), which is mostly covered by seasonal frozen-
322 soil, only has one continuous recession, with K_s = 60d. The results from these two paired
323 catchments provided good reasons to interpret the DBR phenomenon in the Hulu
324 catchment as the result of frozen-soil.

3.3 Perceptual frozen-soil hydrology model of Hulu catchment

326 We did an expert-driven data analysis of the LRET and DBR observations, including time
327 series analysis of precipitation-runoff, soil moisture profile, freeze/thaw depth, and paired
328 catchments comparison. These comprehensive data analyses allowed us to identify that
329 both the LRET and the DBR were the results of frozen-soil, and motivated the following
330 perceptual model (Figure 7).

331 In the freezing season, at local scale, frozen soil occurs from the top soil downwards. But at
332 catchment scale, the freezing process does not occur in a homogeneous way. Since the
333 higher elevation is colder than the lower elevation, the freezing process starts from higher
334 elevation and downwards. At the beginning of the freezing season, although the top soil is
335 already frozen, the groundwater discharge from the supra-permafrost layer still continues. It
336 was found that the groundwater recession from the supra-permafrost layer determines the
337 dominant part of baseflow in permafrost regions (Brutsaert and Sugita, 2008; Ma et al.,
338 2021). Thus, the baseflow recession contributed by both permafrost and seasonal frozen-
339 soil areas, during this period, appears not to be influenced by frozen topsoil, and maintains
340 a linear recession pattern, with K_s=80d in the Hulu catchment.

341 In the frozen season, the hydrological processes in the topsoil are almost completely
342 blocked, although there is still very small amount of unfrozen liquid water in the frozen soil.
343 Thus, surface hydrological processes are almost stopped. With the increase of frozen depth,
344 groundwater in the supra-permafrost layer is frozen gradually from higher to lower
345 elevation, which gradually but dramatically reduces groundwater discharge. Interestingly,
346 permafrost and seasonal frozen-soil have different impacts on baseflow recession. In

347 seasonal frozen-soil region, with shallower frozen depth, the groundwater is still active, and
348 continues the discharge. But in the permafrost region, the groundwater in the supra-
349 permafrost layer is largely inactive. This means the recession, in the frozen periods, was only
350 contributed by the seasonal frozen-soil area, with faster decline of baseflow, and the bend
351 down of hydrograph, with K_s decreased to 60 days in Hulu catchment.

352 During the early thawing season, after a long groundwater recession, the groundwater level
353 is deep; and due to soil evaporation in winter, soil is dry and deficit of moisture.
354 Observations show that with the progress of thawing, soil temperature and soil moisture
355 increase from top to bottom, and the thawing front deepens downward. Rainfall firstly
356 infiltrates to saturate the moisture deficit without runoff generation. Moreover, the existence
357 of the impermeable deeper frozen-soil layer leads to vertical disconnection between soil
358 water and groundwater. Although there is probably saturated water above the frozen soil
359 (Figure 3 and 7), the poor vertical connectivity largely hinders soil water percolation.
360 Without recharge to groundwater, there is limited runoff generation during the early
361 thawing.

362 At the end of the thawing season, as soon as the thaw depth reaches its maximum or
363 frozen-soil no longer exists, the frozen groundwater is released. The spikes in the observed
364 hydrograph are likely due to different parts of the catchment reaching breakthrough, which
365 happens first in the lower elevations and then gradually moves upward to higher landscape
366 elements. This would trigger a sequence of sudden groundwater release and the spikes.
367 Snowfall is probably another influencing factor, causing the LRET and the spikes
368 phenomenon by storing precipitation as snow cover to reduce runoff, and releasing melting
369 water in a short time. This hypothesis needs to be tested by including snow accumulation
370 and melting processes in the hydrological model.

371 Once the soil is completely thawed at the end of the melting season, the rainfall-runoff
372 process returns to normal, and free of influence by the frozen-soil. Hence in the Hulu
373 catchment, frozen soil mainly impacts on streamflow during the freezing, frozen and
374 thawing periods.

375 Based on this perceptual model, we developed the conceptual framework of the frozen-soil
376 hydrological model, which needs to at least to consider the following elements: 1) we need
377 a semi-distributed modeling framework; 2) distributed forcing should be considered. 3)
378 different landscapes should be included; 4) topography should be involved, particularly
379 elevation; 5) we need to consider soil freeze/thaw processes; 6) snowfall and melting should
380 be included; 7) glacier melting should be included; 8) last but not least, the normal rainfall-
381 runoff processes are still important, because most runoff happen in the warm season, which
382 functions the same as in temperate climate regions.

383 4 A semi-distributed conceptual frozen-soil hydrology model

384 The perceptual model requires a quantitative conceptual model to test, revise, polish, verify,
385 or even reject its hypotheses. Since the Hulu catchment has heterogenous landscapes, with

386 a large elevation gradient, diverse land cover, and complex freeze/thaw process, we
387 developed a semi-distributed frozen-soil hydrological model, i.e. FLEX-Topo-FS, based on
388 the landscape-based hydrological modeling framework, i.e. FLEX-Topo. Numerous
389 processes were involved in FLEX-Topo, including the distributed meteorological forcing,
390 landscape heterogeneity, and snow and glacier melting. And in FLEX-Topo-FS, we explicitly
391 considered the impacts of frozen-soil on soil water percolation and groundwater frozen
392 processes in the supra-permafrost layer. The details of both the FLEX-Topo model (without
393 frozen soil) and FLEX-Topo-FS model (with frozen soil) are described in below.

394 4.1 FLEX-Topo model (without frozen-soil)

395 4.1.1 Catchment discretization and meteorological forcing interpolation

396 The FLEX-Topo model classified the entire Hulu catchment into four landscapes, i.e. glaciers,
397 alpine desert, vegetation hillslope, and riparian zone. The Hulu catchment (from 2960m to
398 4820m) was classified into 37 elevation bands, with 50m interval (Figure 2). Combined 4
399 landscapes and 37 elevation bands, we had 37×4=148 hydrological response units (HRUs).
400 The structure of FLEX-Topo model consisted of four parallel components, representing the
401 distinct hydrological function of different landscape elements (Savenije, 2010; Gao et al.,
402 2014; Gharari et al., 2014; Gao et al., 2016). And the corresponding discharge of all elements
403 was subsequently aggregated to obtain the simulated runoff.

404 We interpolated the precipitation (P) and temperature (T) based on elevation bands from
405 in-situ observation (2980m) to each elevation band. The precipitation increasing rate was
406 set as 4.2%/100m, and temperature lapse rate as -0.68°C/100m, based on field
407 measurements (Han et al., 2013). Snowfall (P_s) or rainfall (P_l) was separated by air
408 temperature, with the threshold temperature as 0°C (Gao et al., 2020).

409 4.1.2 Model description and configuration

410 FLEX-Topo is a semi-distributed conceptual bucket model (Savenije, 2010; Gao et al., 2014),
411 with three modules, i.e. the snow and glacier module, the rainfall-runoff module, and the
412 groundwater module. The water balance and constitutive equations can be found in Table 1.
413 The model parameters and their prior ranges for calibration are listed in Table 2.

414 Snow and glacier module

415 The temperature-index method was employed to simulate snow and glacier melting (Gao et
416 al., 2020; He et al., 2021). We used a snow reservoir (S_w) to account for the snow
417 accumulating, melting (M_w) and water balance (Equation 4). The snow degree-day factor
418 (F_{dd}) needs to be calibrated. For glaciers, we assumed its area was constant in our simulation
419 (from 2011 to 2014). Glacier melting (M_g) was also calculated by the temperature-index
420 method (Equation 7), but with different degree-day factor. With the same air temperature,
421 glacier has less albedo than snow cover, thus with larger amount of melting. Glacier
422 degree-factor was obtained by multiplying snow degree-day factor (F_{dd}) with a correct

423   factor C_g (Equation 8) (Gao et al., 2020).

424   **Rainfall-runoff module**

425   There are two reservoirs to simulate rainfall-runoff process, including the root zone
426   reservoir (S_u) (Equation 10) and fast response reservoir (S_f) (Equation 17). To account of the
427   different rainfall-runoff processes in different landscapes and simultaneously avoid over
428   parameterization, we kept the same model structure for vegetation hillslope, riparian and
429   alpine desert (Equation 11, 12), but gave different root zone storage capacity (S_{umax}) values,
430   i.e. S_{umax_R} for riparian, S_{umax_D} for cold desert, and S_{umax_V} for hillslope vegetation. For vegetation
431   hillslope, a larger prior range was constrained for the root zone storage capacity (S_{umax_V}),
432   which means more water is required to fill in its storage capacity to meet its water deficit,
433   which is evidenced by previous studies in this region (Gao et al., 2014). For alpine desert,
434   due to its sparse vegetation cover, we constrained a shallower root zone storage capacity
435   (S_{umax_D}). For the riparian area, due to its location where is prone to be saturated, we also
436   constrained a shallower root zone storage capacity (S_{umax_R}). The initial states (beginning of
437   2011) of the reservoirs were obtained from the end values (end of 2014) of the simulation,
438   which is a normal procedure in modeling practice.

439   Other parameters in rainfall-runoff module (Equation 11-18, Table 1) include the threshold
440   value controlling evaporation (C_e), the shape parameter of the root zone reservoir (β), the
441   splitter (D) separating the generated runoff (R_u) from the root zone reservoir (S_u) to the fast
442   response reservoir, the recession parameter of faster reservoir (K_f), and the lag time from
443   rainfall event to peak flow (T_{lagF}). We set D as 0.2 from the isotope study (Ma et al., 2021).
444   And other parameters to be calibrated, with prior ranges (Table 2) based on previous
445   studies (Gao et al., 2014; Gao et al., 2020).

446   **Groundwater module**

447   The baseflow (Q_s) is generated from groundwater recession. The groundwater was
448   simulated by a linear reservoir (S_s) described in Section 3.2, and Equation 19. We set the
449   prior range for recession coefficient of baseflow reservoir (K_s) as (10-100 d). To estimate the
450   impacts of frozen groundwater on hydrological processes, we set the groundwater in
451   different landscapes as parallel. But we analyzed groundwater level as an integrated system,
452   because groundwater system is connected and this affects the groundwater level. Since the
453   sub-permafrost groundwater is even deeper than 20m in the Hulu catchment, and almost
454   disconnected to streamflow, thus we only model the supra-permafrost groundwater.

455     $$Q_s = S_s / K_s \ (19)$$

456   ## 4.2 FLEX-Topo-FS model (with frozen soil)

457   ### 4.2.1 Modeling the soil freeze/thaw processes

458   FLEX-Topo-FS model employed the Stefan equation (Equation 20), to provide an

459 approximate solution to estimate freeze/thaw depth (Figure 9). The Stefan equation is a
460 temperature-index based freeze-thaw algorithm, which assumes the sensible heat is
461 negligible in soil freeze/thaw simulation (Xie and Gough, 2013). The form of Stefan equation
462 is written as:

463 $\varepsilon = \left(\frac{2 \cdot 86400 \cdot k \cdot F}{Q_L}\right)^{0.5} = \left(\frac{2 \cdot 86400 \cdot k \cdot F}{L \cdot \omega \cdot \rho}\right)^{0.5}$ (20)

464 where ε is the freeze/thaw depth; k is the thermal conductivity (W/(m·K)) of the soil; F is the
465 surface freeze/thaw index. Freeze index (℃ degree-days) is the accumulated negative
466 ground temperature, while freezing; thaw index (℃ degree-days) is accumulated positive
467 ground temperature, while thawing. Q_L is the volumetric latent heat of soil, in J/m^3; and
468 $Q_L = L \cdot \omega \cdot \rho$ where L is the latent heat of fusion of ice (3.35·10^5 J/kg); ω is the water
469 content, as a decimal fraction of the dry soil weight; and ρ is the bulk density of the soil
470 (kg/m^3).

471 We set the thermal conductivity as k=2 W/(m·K), the water content as a decimal fraction of
472 the dry soil weight ω =0.12, and bulk density of the soil ρ=1000 kg/m^3 (Zhang et al.,
473 2019). Since the Stefan equation requires ground surface temperature, which is difficult to
474 measure and often lack of data, we used a multiplier to translate the air temperature to
475 ground temperature. The multiplier during freezing was set as 0.6, and during thawing we
476 assumed the ground surface temperature was the same as air temperature (Gisnås et al.,
477 2016).

478 In this model, we did not consider the impacts of snow cover on soil freeze/thaw, because
479 the snow effects were compiled in the Hulu catchment. Firstly, because precipitation in the
480 Hulu catchment mostly happens in summer as rainfall, and snow depth in the Hulu
481 catchment was less than 10mm in most area and time. Secondly, the snow cover has
482 contrary effects on ground temperature. Snow cover as an isolation layer increased ground
483 temperature in winter. But simultaneously snow cover also increased albedo, which
484 decreased net radiation, and decreased ground temperature. To avoid over
485 parameterization, we did not consider snow effect in the Stefan equation.

486 In this study, the Stefan equation was driven by distributed air temperature, which allowed
487 us to simulate the distributed soil freeze/thaw processes. With the distributed soil freeze
488 index and thaw index, we can also estimate the lower limit of permafrost, of which elevation
489 the freeze index equals to the thaw index in mountainous regions. Field survey on the lower
490 limit of permafrost (Wang et al., 2016) can provide another strong confirmation to our
491 simulated soil freeze/thaw process, except for the spot-scale freeze/thaw depth.

492 **4.2.2 Modeling the impacts of frozen-soil on hydrology**

493 The distributed freeze/thaw status calculated by FLEX-Topo-FS model allowed us to
494 simulate the impacts of frozen-soil on soil and groundwater systems, their connectivity, and
495 eventually catchment runoff.

496 In freezing and frozen seasons, precipitation was in the phase of snowfall, and topsoil was

497   frozen, thus without surface runoff. During this period, runoff is only contributed from the

498   groundwater discharge of the supra-permafrost layer (Q_s). There is no runoff generation (R_u)

499   from the root zone reservoir to the response routine (S_s and S_f) in this period. In the

500   conceptual model, we set $R_u = 0$ (Equation 11). In freezing season, when frozen depth was

501   less than 3m (the depth of active layer in this region), the entire groundwater in the supra-

502   permafrost layer were still connected, and could be simulated by linear groundwater

503   reservoir (S_s). Once the frozen depth of certain elevation zone is larger than 3m, the

504   groundwater in that elevation zone was frozen (F_s). In the FLEX-Topo-FS model, we reduced

505   the groundwater storage (S_s) to 10% of its total storage, to simulate its frozen status

506   (Equation 21, 22). This amount of frozen water (F_s, 90% of groundwater storage when frozen,

507   marked as $S_s(\tilde{t})$) was held in the groundwater system as frozen-soil (Equation 22), but not

508   disappeared. We set 90% frozen, rather than 100%, because there is still unfrozen liquid

509   water in frozen-soil (Romanovsky and Osterkamp, 2000). Groundwater discharge was

510   controlled by the frozen status, which was frozen from high elevations to lower elevations.

511   This process is progressively stopping the function of a series of cascade groundwater

512   buckets, resulting in the discontinuous recession. Simultaneously, the decrease of discharge

513   (Q_s) slowed down the decrease of groundwater level (S_s). This conceptual model allowed us

514   to simulate the bend down of baseflow recession and slower decreasing of groundwater

515   level.

516    $$\frac{\mathrm{d} S_s}{\mathrm{d} t} = R_s - Q_s - F_s \quad (21)$$

517    $$F_s = \begin{cases} 0.9 \cdot S_s(\tilde{t}); & \text{once } \textit{freeze depth} \geq 3m \\ -0.9 \cdot S_s(\tilde{t}); & \text{once } \textit{thaw depth} \text{ reach to yearly max} \\ & \text{or } \textit{thaw depth} \geq \textit{freeze depth} \end{cases} \quad (22)$$

518   In thawing seasons, the freeze/thaw condition in the lowest elevation zone plays a key role,

519   controlling the hydraulic connectivity between soil and groundwater systems. In the

520   conceptual model, if freeze depth calculated by Stefan equation is larger than thaw depth,

521   this means the frozen layer still exists, which obstructs the soil and groundwater connection.

522   In the conceptual model, we kept as the runoff generation $R_u = 0$ (Equation 11). Since there

523   is no percolation from soil to groundwater, and root zone soil moisture (S_u) is accumulating,

524   even ponding in some local depressions (Figure 7). The only outflow of the root zone is

525   evaporation in this period. This conceptual model allowed us to reproduce the LRET

526   observation. For groundwater reservoir, once the thaw depth goes to its yearly maximum (in

527   permafrost area) or thaw depth > freeze depth (in seasonal frozen-soil area), the frozen

528   water (90% of groundwater storage when frozen, $S_s(\tilde{t})$) was released to the groundwater

529   again (Equation 22). The sudden release of frozen groundwater causes the spikes in

530   hydrograph, which could happen in either thawing seasons or complete thaw seasons

531   depending on its elevation. But in either way, the water balance calculation is one-hundred-

532   percent closed.

533   Complete thaw in the lowest elevation marked the end of thawing season, and the start of
534   complete thaw season. In the complete thaw season, soil water and groundwater are
535   connected, and runoff generation (R_u) returns to normal circumstances, which can be
536   simulated by the FLEX-Topo model without frozen-soil.

4.3 Model uncertainty analysis and evaluation metrics

538   The Kling-Gupta efficiency (Gupta et al., 2009; KGE) was used as the performance metric in
539   model calibration:

$$KGE = 1 - \sqrt{(r-1)^2 + (\alpha-1)^2 + (\beta-1)^2} \qquad (23)$$

541   Where r is the linear correlation coefficient between simulation and observation; α ($\alpha =$
542   σ_m/σ_o) is a measure of relative variability in the simulated and observed values, where σ_m is
543   the standard deviation of simulated variables, and σ_o is the standard deviation of observed
544   variables; β is the ratio between the average value of simulated and observed variables.

545   We applied the Generalized Likelihood Uncertainty Estimation framework (GLUE, Beven and
546   Binley, 1992) to estimate model parameter uncertainty. Sampling the parameter space with
547   20, 000 parameter sets, and select the top 1% parameter as behavioral parameter sets.

548   For a comprehensive assessment of model performance in validation, the behavioral model
549   runs were evaluated using multiple criteria, including KGE, KGL (the KGE of logarithms flow,
550   and more sensitive to baseflow), Nash-Sutcliffe Efficiency (NSE) (Nash and Sutcliffe, 1970)
551   (Equation 24), coefficient of determination (R^2) and root mean square error (RMSE).

552    $NSE = 1 - \frac{\sum_{t=1}^{n}(Q_o - Q_m)^2}{\sum_{t=1}^{n}(Q_o - \overline{Q_o})^2}$ (24)

553   Where Q_o is observed runoff, $\overline{Q_o}$ is the observed average runoff, and Q_m is modeled runoff.

554   The model was calibrated in the period 2011-2012, and uses KGE as objective function. The
555   second half time series (2013-2014) were used to quantify the model performance in
556   streamflow split-sample validation, with multi-criteria including KGE, KGL, NSE, R^2, and
557   RMSE. The KGE, KGL, NSE and R^2 are all less than 1, and their valuation closer to 1 indicates
558   better model performance. While the less value of RMSE indicates less error and better
559   performance.

5 Testing the realism of FLEX-Topo-FS model

5.1 FLEX-Topo model results and its discrepancy

562   Figure 10 shows that the FLEX-Topo model can somehow reproduce the observed

563   hydrography in most periods, except for the LRET and DBR events. In calibration, the KGE

564   was 0.78. And in validation, the KGE =0.58, KGL =0.36, NSE =0.41, R^2= 0.82, and RMSE =

565   0.95mm/d. While taking account the impacts of landscape heterogeneity, the FLEX-Topo

566   model can to some extent simulate the LRET phenomenon. The vegetated hillslope in

567   relatively lower elevation has larger unsaturated storage capacity, with larger soil moisture

568   deficit in the beginning of melting season, and capable to hold more rainfall with initial dry

569   soil. Moreover, FLEX-Topo model has took snow accumulation and melting into account,

570   which also reduced the runoff generation during the LRET periods. However, there was still

571   large overestimation in the early thawing season.

572   Additionally, the simulated hydrography on logarithm scale clearly shows that the baseflow

573   is the result of a linear reservoir (Figure 10). The linear reservoir model can mimic recession

574   quite well in the beginning of baseflow recession, but the model discrepancy becomes

575   larger in the middle to the end of frozen season. Hence, FLEX-Topo model is not able to

576   simulate the discontinuous recession. The model discrepancy indicates that without

577   considering frozen-soil, FLEX-Topo cannot well reproduce the observed LRET and DBR

578   observations, although explicitly considered landscape heterogeneity, snow and glacier

579   processes.

580   ## 5.2 FLEX-Topo-FS model results

581   ### 5.2.1 Freeze/thaw simulation by FLEX-Topo-FS model

582   Figure 9 demonstrates that the Stefan equation was capable to reproduce the freeze/thaw

583   process. This verified the success of the freeze/thaw parameterization and the parameter

584   sets. Also, the simulated lower limit of permafrost is 3716m, which is largely close to field

585   survey in the upper Heihe River basin, around 3650 – 3700 m (Wang et al., 2016), and the

586   expert-based estimation of 3650 m of Hulu catchment. Both the well reproduced

587   freeze/thaw variation in spot scale, and the lower limit of permafrost in catchment scale,

588   gave us strong confidence to the simulation of soil freeze/thaw processes.

589   ### 5.2.2 Runoff simulation by FLEX-Topo-FS model

590   While considering the impacts of frozen-soil, the FLEX-Topo-FS model, compared with

591   FLEX-Topo, dramatically improved the model performance. Figure 10 showed the simulated

592   hydrograph by FLEX-Topo-FS on both normal and log scales. Both the LRET and the DBR

593   observations were almost perfectly reproduced by the FLEX-Topo-FS model. The KGE of

594   FLEX-Topo-FS in calibration was 0.78, which was the same as FLEX-Topo. But in validation,

595   the performance was significantly improved, the KGE improved from 0.58 to 0.66, KGL was

596   from 0.36 to 0.72, NSE was from 0.41 to 0.60, R^2 from 0.82 to 0.83, and RMSE was reduced

597   from 0.95mm/d to 0.79mm/d. All the model evaluation criteria were improved. The most

598   significant improvement was the baseflow simulation, and KGL was increased from 0.36 to

599   0.72. We also noted that the FLEX-Topo-FS model reproduced the spikes during the

600   thawing in Figure 10. This further confirms our conceptual model of a sequence of thawing

601 breakthroughs, which trigger the sudden release of groundwater starting at lower elevations
602 and progressing to higher landscape elements.

603 5.2.3 Modeling groundwater trends

604 To further verify the FLEX-Topo-FS model, we averaged the simulated groundwater storage
605 (S_s) of all HRUs, and compared with the observed groundwater depth on log scale (Figure
606 11). We included the frozen groundwater in the total groundwater storage (S_s), because the
607 liquid groundwater is in connection with the frozen groundwater and this affects the
608 groundwater level variation. Figure 11 clearly demonstrated that the simulated groundwater
609 storage decreased slower, and the time scale of recession was increased. The trends of
610 simulated groundwater storage and observed groundwater level, which are not the same,
611 but similar physical meaning describing groundwater dynamic, correspond surprisingly well.
612 This is particularly encouraging, given that the periods of simulation (2011-2014) and
613 observation (2016-2019) were not overlaid, and a point observation may not be
614 straightforwardly representative for the entire basin.

615 The success to reproduce groundwater level trends is another strong confirmation for the
616 FLEX-Topo-FS model. All the successes of FLEX-Topo-FS model to reproduce spot scale
617 freeze/thaw depth variation, lower limit of permafrost, LRET and DBR events, and
618 groundwater level trends, gave us strong confidence to the realism of our qualitative
619 perceptual model and quantitative conceptual model.

620 # 6 Discussion

621 ## 6.1 Diagnosing the impacts of frozen-soil on complex mountainous hydrology

622 ### 6.1.1 Understanding complex frozen-soil hydrology by hydrography analysis

623 Frozen-soil happens underneath, with frustrating spatial-temporal heterogeneities, and
624 difficulty to measure. Although there are spot and hillslope measurements, its impact on
625 catchment hydrology is still hard to explore. Hydrography, easily and widely observed and
626 globally accessible, can be regarded as the by-product of the entire catchment hydrological
627 system (Gao, 2015). Hydrography as an integrated signal provides us a vital source of
628 information, reflecting how the complex hydrological system works, i.e. transforming
629 precipitation into runoff. Hence, hydrography itself is a valuable source of data to
630 understand catchment frozen-soil hydrology.

631 Especially the baseflow embodies the influence of basin characteristics including the
632 geology, soils, morphology, vegetation, and frozen-soil (Blume et al., 2007; Ye et al., 2009).
633 Hence, the quantitative description of baseflow is a valuable tool for understanding how the
634 groundwater system behaves (McNamara et al., 1998). Baseflow recession was used to
635 identify the impacts of climate change on permafrost hydrology. In previous studies,
636 Slaughter and Kane (1976) found that basins with permafrost have higher peak flows and

637   lower baseflows. The baseflow, representing groundwater recession, provides important
638   information about the storage capacity and recession characteristics of the active layer in
639   permafrost regions (Brutsaert, and Hiyama, 2012).

640   Moreover, hydrological system has tremendous influencing factors. The hydrograph of
641   paired catchments provides a good reference, as a controlled experiment, to isolate one
642   influencing factor from the others. Nested catchments helped us to acknowledge the
643   importance of region-specific knowledge, which is often the key to interpret the
644   unexplained variability of large sample studies (Fenicia and McDonnell, 2022). In this study,
645   the pair catchment method helped us to confirm the impacts of frozen-soil on LRET and
646   DBR observations.

647   Additionally, by analyzing the nested sub-basins of the Lena River in Siberia, Ye et al. (2008)
648   used the peak flow/baseflow ratio to quantify the impact of permafrost coverage on
649   hydrograph regime in Lena River basin, and found that frozen-soil only affects discharge
650   regime over high permafrost regions (greater than 60%), and no significant affect over the
651   low permafrost (less than 40%) regions. In this study, we reconfirmed this statement. The
652   permafrost area proportions of the Hulu catchment and Zhamashike sub-basin are 64% and
653   74%, with significant effects on discharge, while 38% of the Qilian sub-basin is covered by
654   permafrost, with no significant effects on discharge regime.

655   By paired catchments comparison, interestingly, the K_s in Zhamashike and Qilian in the early
656   recession period are both 60d, which is exactly within the standard value of 45±15 days
657   derived in earlier studies for basins ranging in size between 1,000 and 100,000 km^2
658   (Brutsaert and Sugita, 2008; Brutsaert and Hiyama, 2012), which was likely the results of
659   catchment self-similarity and co-evolution. But we also noticed that the K_s in the small Hulu
660   catchment (K_s = 80d and 60d) is quite larger than the Zhamashike (K_s = 60d and 20d) and
661   Qilian (K_s = 60d). This could be rooted in different scale and drainage density (Brutsaert and
662   Hiyama, 2012). The Hulu catchment is located in the headwater with less drainage density,
663   hence less contact area between hillslope and river channel, slower baseflow recession, and
664   larger K_s value. We argue that even without the impacts from frozen-soil, it is difficult to
665   give accurate K_s estimation in small catchments (less than 1,000 km^2) in moderate climates. It
666   is more substantial difficult to estimate the discontinuous K_s in different periods in frozen-
667   soil catchments without calibration. Thus, estimating the value of recession coefficient (K_s) in
668   different catchments and periods, especially for small catchments and in cold regions, is still
669   an intriguing scientific question for hydrologists.

670   **6.1.2 Understanding complex frozen-soil hydrology by multi-source observations**

671   Observation is still a bottleneck in complex mountainous cold regions. Traditionally,
672   fragmented observations are only for specific variables, like puzzles. In this study, we
673   collected multi-source data, including soil moisture, groundwater level, topography,
674   geology survey, isotope, soil temperature, freeze/thaw depth, permafrost and seasonal
675   frozen-soil map, and hydrograph in paired catchments. Multi-source data analysis provides
676   multi-dimensional perspective to investigate frozen-soil hydrology. We argue that on one
677   hand, multi-source observations helped us to deliver the perceptual and conceptual

678 models. And on the other hand, perceptual and conceptual models bridge the gap between
679 experimentalists and modelers (Seibert and McDonnell, 2002), allowing us put fragmented
680 observations together, and understand the hydrological system in an integrated and
681 qualitative way.

682 Data gap is a common issue in mountainous hydrology studies. For example, in this study,
683 runoff data has a gap period in the end of thawing season in 2013, due to flooding and
684 equipment malfunction. Soil moisture and groundwater level data had large gap, which
685 cannot be used for continuous modeling. Luckily, the meteorological data, which is
686 important forcing data to run the models, was continuous without any gap. With sufficient
687 meteorological forcing data, we successfully run the hydrological models from 2011 to
688 2014. The runoff data gap in the end of thawing season in 2013 merely influenced model
689 validation. While evaluating models, we did not involve the data gap period. Hence, the
690 data gap does not have any impact on the consolidation of the conclusions.

691 Although soil moisture had large gap, fortunately there were some observations during the
692 LRET periods, which were sufficient to distinguish the impacts of frozen soil on soil moisture
693 profile. Additionally, although the groundwater level observation (2016-2019) was not
694 overlaid with other hydrometeorological measurements (2011-2014), its repeating seasonal
695 pattern allowed us to qualitatively understand how groundwater system behaves.
696 Groundwater fluctuation in natural catchments has strong periodicity, which can be
697 observed in Figure 11. Groundwater variation does not show significant difference among
698 different years, which is especially true for the 25m well. Due to the extreme difficulty of
699 continuous observation in this region, there was no groundwater measurement in 2011-
700 2014. But due to the strong repeated temporal variation of groundwater level, we have
701 good reason to believe the trends in 2016-2019 also happened in 2011-2014. Moreover,
702 this is a qualitative comparison, rather than a quantitative one, which we do not think has
703 any impact on our conclusions.

704 In general, we argue that data gap always exists. In another words, we can never have
705 sufficient data. The only thing we can do is using the accessible data to understand
706 processes. Although perfect data does not exist, with more multi-source and better data
707 quality, the more accurate understanding we can achieve. This needs the close collaboration
708 among multi-disciplinary researchers, including but not limited to hydrologists,
709 meteorologists, ecologists, geocryologists, geologists, and engineers.

710 **6.1.3 Understanding complex frozen-soil hydrology by model discrepancy**

711 By a simple water balance inspection, we found that the total annual runoff of Hulu
712 catchment was 499mm/a, which is even larger than the observed annual precipitation
713 433mm/a. This means that without considering distributed meteorological forcing, the
714 runoff coefficient is larger than 1, and the water balance cannot be closed. This result is also
715 in line with previous studies, showing that precipitation in mountainous areas is largely
716 underestimated (Immerzeel et al., 2015; Chen et al., 2018; Zhang et al., 2018b).

717 Although the semi-distributed FLEX-Topo has considered tremendous processes, including

718 rainfall-runoff processes, distributed forcing, landscape heterogeneity, topography, snow
719 and glacier melting, there was still model discrepancy to reproduce the LRET and DBR
720 observations. This means there must be some processes missed in the model. After our
721 expert-driven data analysis, we attributed the model discrepancy to soil freeze/thaw
722 processes.

723 Model fitness is the goal which all modelers are pursuing. But we argue that in many cases,
724 model discrepancy can tell us more interesting things than perfect fitting. In this study, we
725 used the FLEX-Topo model, without frozen-soil, as a diagnosing tool to understand the
726 possible impacts of frozen-soil on the complex mountainous hydrology. Using tailor-made
727 hydrological model and integrated observations as diagnostic tools is a promising approach
728 to step-wisely understand the complex mountainous hydrology.

6.2 Modeling frozen-soil hydrology: top-down VS bottom-up

730 Top-down and bottom-up are two philosophies for model development (Sivalpalan et al.,
731 2003). The bottom-up approach attempts to model catchment scale response based on the
732 prior knowledge learned in small scale. Bottom-up approach is commonly used in frozen-
733 soil hydrological modeling, because this is straightforward. And for modeling, it is a
734 common practice to experiment with/without a certain process, and claim its impacts on
735 runoff. But the bottom-up modeling largely missed the key step to diagnose the impacts of
736 small-scale processes on catchment response. Lack of process understanding usually leads
737 modeling studies to data pre- and pro-processing and extensive parameter calibration with
738 the risk of equifinality and model malfunction.

739 By our expert-driven top-down modeling approach, we firstly tried to understand the
740 hydrological processes at work, using multi-source data and analysing model discrepancy.
741 We then translated our understanding to perceptual and conceptual models. The top-down
742 method is an appealing way to identify the key influencing factors, rather than being lost in
743 endless details and heterogeneities. Such informed analysis of the data helps to bring
744 experimentalist insights into the initiation of the conceptual model construction.

6.3 Warming impacts on frozen-soil hydrology

746 To quantify the impacts of warming on frozen-soil hydrology, we arbitrarily set the air
747 temperature increased by 2°C. The FLEX-Topo-FS simulation illustrated that complete thaw
748 date became 16-19 days earlier, and the lower limit of permafrost increased by 294 m, from
749 3716m to 4010m. For runoff simulation, the DBR phenomenon became less obvious (Figure
750 12). This is because two-degree warming results in permafrost degradation, which means
751 most permafrost is degraded to seasonal frozen-soil. Since the DBR was caused by the
752 different groundwater discharge behaviors in permafrost and seasonal frozen-soil areas.
753 Specially, the first recession period was contributed by the groundwater discharge from
754 both permafrost and seasonal frozen-soil areas, and the second recession period was only
755 from the seasonal frozen-soil area. The permafrost degradation turns most permafrost into

756 seasonal frozen-soil, and makes groundwater discharge nearly only from the seasonal
757 frozen-soil region, and leads to more continuous baseflow recession. Eventually, warming
758 leads to the increase of both the baseflow and runoff in early thawing seasons. The warming
759 effect on baseflow was already widely observed in Arctic and mountainous permafrost rivers
760 (Ye et al., 2009; Brutsaert et al., 2012; Niu et al., 2010; Song et al., 2020). Hence, these wide
761 observations could be another verification for the FLEX-Topo-FS model realism. For
762 implications in water resource management, the results indicate that frozen soil degradation
763 caused by climate change may largely alter streamflow regime, especially for the thirsty
764 spring and early summer, in vast cold QTP. It is also worthwhile to be noted that this is
765 primary prediction. We used 2 degrees warmer more like using a sensitive analysis to
766 illustrate how warming will impact on baseflow, to further verify the capability and
767 robustness of the model itself. In future studies, we need more detailed modelling studies to
768 use the state-of-the-art climate prediction and downscaling methodologies, to assess the
769 frozen-soil change and hydrology variations.

6.4 Implications for other cold regions

771 We believe that the FLEX-Topo-FS model has great potential to be applied in other cold
772 regions. There are mainly three reasons.

773 Firstly, our study site, the Hulu catchment, although small (23.1 km^2), has a large elevation
774 gradient (from 2960 m to 4820 m), diverse landscapes (hillslope vegetation, riparian area,
775 alpine desert, and glaciers), snowfall and snowmelt, and both permafrost and seasonal
776 frozen-soil. Our newly developed model explicitly considered all these spatial and temporal
777 heterogeneities, and eventually achieved excellent performance. With such a comprehensive
778 modeling toolkit, the model has potential to be upscaled or transfer to other cold regions.

779 Secondly, we obtained the perceptual model from not only the observations and our expert
780 knowledge at the Hulu catchment itself, but also widely considered the impact of frozen-
781 soil on hydrological processes in other catchments, including the Zhamashike and Qilian
782 (two nested sub-catchments of the upper Heihe), the headwater of Yellow River, and the
783 Cape Bounty Arctic Watershed Observatory in Canada. Thus, we developed the model for
784 the Hulu catchment in the context of larger scale observations.

785 Thirdly, the realism of the conceptual model was confirmed not only by streamflow
786 measurement, but also by multi-source and multi-scale observations, particularly the
787 freezing and thawing front in the soil, the lower limit of permafrost, and the trends in
788 groundwater level variation.

789 Although our new model generally has great potential to be used in other cold regions, we
790 should be cautious to arbitrarily use the model without any prior understanding of the
791 modeling system. Since frozen-soil is merely one influential factor for cold region
792 hydrology, there are other factors having notable impacts, which are intertwined with
793 frozen-soil. This relates especially to the geology condition, which can have considerable
794 impact on frozen-soil, but has large spatial heterogeneity, and where it is difficult to take
795 measurements. For the model empirical parameters, most of them are related to the freeze-

thaw processes related to Stefan equation, which have clear physical meanings, and confirmed by previous studies with a good spatial distribution over the entire QTP (e.g. Zou et al., 2017; Ran et al., 2022). Due to the extreme complexity of soil and geology in mountainous catchment, we still need to recalibrate their values while modeling other basins on the QTP. Hence, before upscaling to other cold regions, we recommend to follow a stringent modeling procedure, i.e expert-driven data analysis → qualitative perceptual model → quantitative conceptual model → testing of model realism.

7 Conclusions

Our knowledge on frozen-soil hydrology is still incomplete, which is particularly true for complex mountainous catchment on the QTP. In the past decades, we have collected numerous heterogeneities and complexities in frozen-soil regions, but most of these observations are still neither well integrated into hydrological models, nor used to constrain model structure or parameterization in catchment-scale studies. More importantly, we still largely lack quantitative knowledge on which variables play more dominant roles at certain spatial-temporal scales, and should be included in models with priority.

By conducting this frozen-soil hydrological modeling study for the complex mountainous Hulu catchment, we reached the following conclusions: 1) we observed two new phenomena in the frozen-soil catchment, i.e. the low runoff in early thawing seasons (LRET) and discontinuous baseflow recession (DBR), which are widespread but not yet reported; 2) without considering the frozen-soil, the FLEX-Topo model was not able to reproduce LRET and DBR observations; 3) considering frozen-soil impacts on soil-groundwater connectivity, and groundwater recession, the FLEX-Topo-FS model successfully reproduced the LRET and DBR events. The FLEX-Topo-FS results were also verified by observed freeze/thaw depth variation, groundwater level, and lower limit of permafrost. We believe this study is able to give us new insights into further implications to understand the impact of frozen soil on hydrology, projecting the impacts of climate change on water resources in vast cold regions, which is one of the 23 major unsolved scientific problems in hydrology community.

ACKNOWLEDGMENTS

We thank two anonymous reviewers for their constructive comments and suggestions, which helped us to improve the paper. This study was supported by the National Natural Science Foundation of China (Grant Nos. 42122002, 42071081, 42171125, and 41971041).

References:

Andresen, C. G., Lawrence, D. M., Wilson, C. J., David McGuire, A., Koven, C., Schaefer, K., Jafarov, E., Peng, S., Chen, X., Gouttevin, I., Burke, E., Chadburn, S., Ji, D., Chen, G., Hayes, D.

832   and Zhang, W.: Soil moisture and hydrology projections of the permafrost region-a model

833   intercomparison, Cryosphere, 14(2), 445–459, doi:10.5194/tc-14-445-2020, 2020.

834   Beven, K. and Binley, A.: The future of distributed models: Model calibration and uncertainty

835   prediction, Hydrol. Process., 6(3), 279–298, doi:10.1002/hyp.3360060305, 1992.

836   Blume, T., Zehe, E. and Bronstert, A.: Rainfall-runoff response, event-based runoff

837   coefficients and hydrograph separation, Hydrol. Sci. J., 52(5), 843–862,

838   doi:10.1623/hysj.52.5.843, 2007.

839   Blöschl, G., Bierkens, M. F. P., Chambel, A., et al.: Twenty-three unsolved problems in

840   hydrology (UPH)–a community perspective, Hydrol. Sci. J., 64(10), 1141–1158,

841   doi:10.1080/02626667.2019.1620507, 2019.

842   Bring, A., Fedorova, I., Dibike, Y., Hinzman, L., Mård, J., Mernild, S. H., Prowse, T., Semenova,

843   O., Stuefer, S. L. and Woo, M. K.: Arctic terrestrial hydrology: A synthesis of processes,

844   regional effects, and research challenges, J. Geophys. Res. G Biogeosciences, 121(3), 621–

845   649, doi:10.1002/2015JG003131, 2016.

846   Brutsaert, W. and Sugita, M.: Is Mongolia's groundwater increasing or decreasing? The case

847   of the Kherlen River basin, Hydrol. Sci. J., 53(6), 1221–1229, doi:10.1623/hysj.53.6.1221,

848   2008.

849   Brutsaert, W. and Hiyama, T.: The determination of permafrost thawing trends from long-

850   term streamflow measurements with an application in eastern Siberia, J. Geophys. Res.

851   Atmos., 117(22), 1–10, doi:10.1029/2012JD018344, 2012.

852   Bui, M. T., Lu, J. and Nie, L.: A review of hydrological models applied in the permafrost-

853   dominated Arctic region, Geosci., 10(10), 1–27, doi:10.3390/geosciences10100401, 2020.

854   Cao, B., Zhang, T., Wu, Q., Sheng, Y., Zhao, L. and Zou, D.: Permafrost zonation index map

855   and statistics over the Qinghai–Tibet Plateau based on field evidence, Permafr. Periglac.

856   Process., 30(3), 178–194, doi:10.1002/ppp.2006, 2019.

857   Chadburn, S., Burke, E., Essery, R., Boike, J., Langer, M., Heikenfeld, M., Cox, P. and

858   Friedlingstein, P.: An improved representation of physical permafrost dynamics in the JULES

859   land-surface model, Geosci. Model Dev., 8(5), 1493–1508, doi:10.5194/gmd-8-1493-2015,

860   2015.

861   Chang, J., Wang, G. X., Li, C. J. and Mao, T. X.: Seasonal dynamics of suprapermafrost

862   groundwater and its response to the freeing-thawing processes of soil in the permafrost

863   region of Qinghai-Tibet Plateau, Sci. China Earth Sci., 58(5), 727–738, doi:10.1007/s11430-

864   014-5009-y, 2015.

865   Chen, R., Song, Y., Kang, E., Han, C., Liu, J., Yang, Y., Qing, W. and Liu, Z.: A cryosphere-

866   hydrology observation system in a small alpine watershed in the Qilian mountains of China

867   and its meteorological gradient, Arctic, Antarct. Alp. Res., 46(2), 505–523, doi:10.1657/1938-

868   4246-46.2.505, 2014.

869   Chen, R., Wang, G., Yang, Y., Liu, J., Han, C., Song, Y., Liu, Z. and Kang, E.: Effects of

Cryospheric Change on Alpine Hydrology: Combining a Model With Observations in the Upper Reaches of the Hei River, China, J. Geophys. Res. Atmos., 123(7), 3414–3442, doi:10.1002/2017JD027876, 2018.

Chiasson-Poirier, G., Franssen, J., Lafrenière, M. J., Fortier, D. and Lamoureux, S. F.: Seasona evolution of active layer thaw depth and hillslope-stream connectivity in a permafrost watershed, Water Resour. Res., 56(1), 1–18, doi:10.1029/2019WR025828, 2020.

Cuo, L., Zhang, Y., Bohn, T. J., Zhao, L., Li, J., Liu, Q. and Zhou, B.: Journal of geophysical research, Nature, 175(4449), 238, doi:10.1038/175238c0, 1955.

Ding, Y., Zhang, S., Chen, R., Han, T., Han, H., Wu, J., Li, X., Zhao, Q., Shangguan, D., Yang, Y., Liu, J., Wang, S., Qin, J. and Chang, Y.: Hydrological Basis and Discipline System of Cryohydrology: From a Perspective of Cryospheric Science, Front. Earth Sci., 8(December), doi:10.3389/feart.2020.574707, 2020.

Dobinski, W.: Permafrost. Earth-Science Reviews, 108, 158–169, 2011.

Evans, S. G., Ge, S., Voss, C. I. and Molotch, N. P.: The Role of Frozen Soil in Groundwater Discharge Predictions for Warming Alpine Watersheds, Water Resour. Res., 54(3), 1599–1615, doi:10.1002/2017WR022098, 2018.

Fabre, C., Sauvage, S., Tananaev, N., Srinivasan, R., Teisserenc, R. and Pérez, J. M. S.: Using modeling tools to better understand permafrost hydrology, Water (Switzerland), 9(6), doi:10.3390/w9060418, 2017.

Farquharson, L. M., Romanovsky, V. E., Cable, W. L., Walker, D. A., Kokelj, S. V. and Nicolsky, D.: Climate Change Drives Widespread and Rapid Thermokarst Development in Very Cold Permafrost in the Canadian High Arctic, Geophys. Res. Lett., 46(12), 6681–6689, doi:10.1029/2019GL082187, 2019.

Fenicia, F., Savenije, H. H. G., Matgen, P. and Pfister, L.: Is the groundwater reservoir linear? Learning from data in hydrological modelling, Hydrol. Earth Syst. Sci., 10(1), 139–150, doi:10.5194/hess-10-139-2006, 2006.

Fenicia, F., Kavetski, D. and Savenije, H. H. G.: Elements of a flexible approach for conceptual hydrological modeling: 1. Motivation and theoretical development, Water Resour. Res., 47(11), 1–13, doi:10.1029/2010WR010174, 2011.

Fenicia, F. and McDonnell, J. J.: Modeling streamflow variability at the regional scale: (1) perceptual model development through signature analysis, J. Hydrol., 605(December 2021), 127287, doi:10.1016/j.jhydrol.2021.127287, 2022.

Gao, B., Yang, D., Qin, Y., Wang, Y., Li, H., Zhang, Y. and Zhang, T.: Change in frozen soils and its effect on regional hydrology, upper Heihe basin, northeastern Qinghai-Tibetan Plateau, Cryosphere, 12(2), 657–673, doi:10.5194/tc-12-657-2018, 2018.

Gao, H., Hrachowitz, M., Fenicia, F., Gharari, S. and Savenije, H. H. G.: Testing the realism of a topography-driven model (FLEX-Topo) in the nested catchments of the Upper Heihe, China, Hydrol. Earth Syst. Sci., 18(5), 1895–1915, doi:10.5194/hess-18-1895-2014, 2014.

908 Gao, H.: Landscape-based hydrological modelling: understanding the influence of climate,
909 topography, and vegetation on catchment hydrology, Ph.D. Dissertation, Delft University of
910 Technology, 2015

911 Gao, H., Hrachowitz, M., Sriwongsitanon, N., Fenicia, F., Gharar, S.i, and Savenije, H. H. G.:
912 Water Resources Research, J. Am. Water Resour. Assoc., 5(3), 2–2, doi:10.1111/j.1752-
913 1688.1969.tb04897.x, 1969.

914 Gao, H., Ding, Y., Zhao, Q., Hrachowitz, M. and Savenije, H. H. G.: The importance of aspect
915 for modelling the hydrological response in a glacier catchment in Central Asia, Hydrol.
916 Process., 31(16), 2842–2859, doi:10.1002/hyp.11224, 2017.

917 Gao, H., Dong, J., Chen, X., Cai, H., Liu, Z., Jin, Z., Mao, D., Yang, Z. and Duan, Z.: Stepwise
918 modeling and the importance of internal variables validation to test model realism in a data
919 scarce glacier basin, J. Hydrol., 591(September), 125457, doi:10.1016/j.jhydrol.2020.125457,
920 2020.

921 Gao, H., Wang, J., Yang, Y., Pan, X., Ding, Y. and Duan, Z.: Permafrost Hydrology of the
922 Qinghai-Tibet Plateau: A Review of Processes and Modeling, Front. Earth Sci., 8(January),
923 doi:10.3389/feart.2020.576838, 2021.

924 Gao, J., Xie, Z., Wang, A., Liu, S., Zeng, Y., Liu, B., Li, R., Jia, B., Qin, P. and Xie, J.: A New
925 Frozen Soil Parameterization Including Frost and Thaw Fronts in the Community Land
926 Model, J. Adv. Model. Earth Syst., 11(3), 659–679, doi:10.1029/2018MS001399, 2019.

927 Gharari, S., Hrachowitz, M., Fenicia, F., Gao, H. and Savenije, H. H. G.: Using expert
928 knowledge to increase realism in environmental system models can dramatically reduce the
929 need for calibration, Hydrol. Earth Syst. Sci., 18(12), 4839–4859, doi:10.5194/hess-18-4839-
930 2014, 2014.

931 Gisnas, K., Westermann, S., Vikhamar Schuler, T., Melvold, K. and Etzelmüller, B.: Small-scale
932 variation of snow in a regional permafrost model, Cryosphere, 10(3), 1201–1215,
933 doi:10.5194/tc-10-1201-2016, 2016.

934 Gouttevin, I., Krinner, G., Ciais, P., Polcher, J. and Legout, C.: Multi-scale validation of a new
935 soil freezing scheme for a land-surface model with physically-based hydrology, Cryosphere,
936 6(2), 407–430, doi:10.5194/tc-6-407-2012, 2012.

937 Gupta, H. V., Kling, H., Yilmaz, K. K. and Martinez, G. F.: Decomposition of the mean squared
938 error and NSE performance criteria: Implications for improving hydrological modelling, J.
939 Hydrol., 377(1–2), 80–91, doi:10.1016/j.jhydrol.2009.08.003, 2009.

940 Han, C., Chen, R., Liu, J., Yang, Y., Liu, Z.: Hydrological characteristics in non-freezing period
941 at the alpine desert zone of Hulugou watershed, Qilian Mountains. Journal of Glaciology
942 and Geocryology, 35(6), 1536-1544, 2013.

943 Han, C., Chen, R., Liu, Z., Yang, Y., Liu, J., Song, Y., Wang, L., Liu, G., Guo, S. and Wang, X.:
944 Cryospheric Hydrometeorology Observation in the Hulu Catchment (CHOICE), Qilian
945 Mountains, China, Vadose Zo. J., 17(1), 180058, doi:10.2136/vzj2018.03.0058, 2018.

He, Z., Duethmann, D. Tian, F. A meta-analysis based review of quantifying the contributions of runoff components to streamflow in glacierized basins. Journal of Hydrology, 603, 126890, 2021

Hülsmann, L., Geyer, T., Schweitzer, C., Priess, J. and Karthe, D.: The effect of subarctic conditions on water resources: initial results and limitations of the SWAT model applied to the Kharaa River Basin in Northern Mongolia, Environ. Earth Sci., 73(2), 581–592, doi:10.1007/s12665-014-3173-1, 2015.

Immerzeel, W. W., Van Beek, L. P. H. and Bierkens, M. F. P.: Climate change will affect the asian water towers, Science (80-.)., 328(5984), 1382–1385, doi:10.1126/science.1183188, 2010.

Immerzeel, W. W., Wanders, N., Lutz, A. F., Shea, J. M. and Bierkens, M. F. P.: Reconciling high-altitude precipitation in the upper Indus basin with glacier mass balances and runoff, Hydrol. Earth Syst. Sci., 19(11), 4673–4687, doi:10.5194/hess-19-4673-2015, 2015.

Jarvis PG.: Prospects for bottom-up models. In Scaling Physiological Processes: Leaf to Globe. Ehleringer JR, Field CB (eds). Academic Press, 1993.

Jiang, H., Zheng, G., Yi, Y., Chen, D., Zhang, W., Yang, K. and Miller, C. E.: Progress and Challenges in Studying Regional Permafrost in the Tibetan Plateau Using Satellite Remote Sensing and Models, Front. Earth Sci., 8(December), doi:10.3389/feart.2020.560403, 2020.

Krogh, S. A., Pomeroy, J. W. and Marsh, P.: Diagnosis of the hydrology of a small Arctic basin at the tundra-taiga transition using a physically based hydrological model, J. Hydrol., 550(May), 685–703, doi:10.1016/j.jhydrol.2017.05.042, 2017.

Kurylyk, B. L., M. Hayashi, W. L. Quinton, J. M. McKenzie, and C. I. Voss: Influence of vertical and lateral heat transfer on permafrost thaw, peatland landscape transition, and groundwater flow, Water Resour. Res., 52, 1286–1305, doi:10.1002/2015WR018057, 2016.

Lafrenière, M. J., and Lamoureux, S. F.: Effects of changing permafrost conditions on hydrological processes and fluvial fluxes. Earth-Science Reviews, 191, 212–223, 2019.

Li, X., Wu, T., Zhu, X., Jiang, Y., Hu, G., & Hao, J., et al.: Improving the Noah-MP model for simulating hydrothermal regime of the active layer in the permafrost regions of the Qinghai-Tibet Plateau. Journal of Geophysical Research: Atmospheres, 125, e2020JD032588. https://doi.org/10.1029/2020JD032588, 2020

Lindstrom, G., Bishop, K., and Lofvenius, M. O.: Soil frost and runoff at Svartberget, northern Sweden—measurements and model analysis. Hydrol. Process. 16, 3379–3392, 2002

Liu, Y., Zhao, L., and Li, R.: Simulation of the soil water-thermal features within the active layerin Tanggula region, Tibetan plateau, by using SHAW model. J. Glaciol. Geocryol. 35, 280–290, 2013

Lyon, S. W., Destouni, G., Giesler, R., Humborg, C., Mörth, M., Seibert, J., Karlsson, J. and Troch, P. A.: Estimation of permafrost thawing rates in a sub-arctic catchment using recession flow analysis, Hydrol. Earth Syst. Sci., 13(5), 595–604, doi:10.5194/hess-13-595-

984   2009, 2009.

985   Ma, R., Sun, Z., Hu, Y., Chang, Q., Wang, S., Xing, W. and Ge, M.: Hydrological connectivity
986   from glaciers to rivers in the Qinghai-Tibet Plateau: Roles of suprapermafrost and
987   subpermafrost groundwater, Hydrol. Earth Syst. Sci., 21(9), 4803–4823, doi:10.5194/hess-
988   21-4803-2017, 2017.

989   Ma, R., Sun, Z., Chang, Q., Ge, M., Pan, Z.: Control of the interactions between stream and
990   groundwater by permafrost and seasonal frost in an alpine catchment, northeastern Tibet
991   Plateau, China. Journal of Geophysical Research: Atmospheres, 126, e2020JD033689, 2021

992   McNamara, J. P., Kane, D. L. and Hinzman, L. D.: An analysis of streamflow hydrology in the
993   Kuparuk River Basin, Arctic Alaska: A nested watershed approach, J. Hydrol., 206(1–2), 39–
994   57, doi:10.1016/S0022-1694(98)00083-3, 1998.

995   Muster, S., Langer, M., Heim, B., Westermann, S. and Boike, J.: Subpixel heterogeneity of ice-
996   wedge polygonal tundra: A multi-scale analysis of land cover and evapotranspiration in the
997   Lena River Delta, Siberia, Tellus, Ser. B Chem. Phys. Meteorol., 64(1), 0–19,
998   doi:10.3402/tellusb.v64i0.17301, 2012.

999   Nash, J. and Sutcliffe, J.V.: River Flow Forecasting through Conceptual Models Part I—A
1000   Discussion of Principles. Journal of Hydrology, 10, 282-290,
1001   http://dx.doi.org/10.1016/0022-1694(70)90255-6, 1970

1002   Nyberg, L.: Soil frost effects on soil water and runoff dynamics along a boreal forest
1003   transect: 1. Field investigations. Hydrol. Process. 15, 909–926, 2001.

1004   Niu, G. Y. and Yang, Z. L.: Effects of frozen soil on snowmelt runoff and soil water storage at
1005   a continental scale, J. Hydrometeorol., 7(5), 937–952, doi:10.1175/JHM538.1, 2006.

1006   Niu L, Ye B S, Li J, et al.: Effect of permafrost degradation on hydrological processes in
1007   typical basins with various permafrost coverage in Western China. Sci China Earth Sci, doi:
1008   10.1007/s11430-010-4073-1, 2010.

1009   Nitze, I., Grosse, G., Jones, B. M., Romanovsky, V. E. and Boike, J.: Remote sensing quantifies
1010   widespread abundance of permafrost region disturbances across the Arctic and Subarctic,
1011   Nat. Commun., 9(1), 1–11, doi:10.1038/s41467-018-07663-3, 2018.

1012   Oleson, K. and Lawrence, D.: NCAR / TN-503 + STR NCAR Technical Note July 2013
1013   Technical Description of version 4 . 5 of the Community Land Model (CLM), (March 2014),
1014   2013.

1015   Osuch, M., Wawrzyniak, T. and Nawrot, A.: Diagnosis of the hydrology of a small Arctic
1016   permafrost catchment using HBV conceptual rainfall-runoff model, Hydrol. Res., 50(2), 459–
1017   478, doi:10.2166/nh.2019.031, 2019.

1018   Pan, X., Li, Y., Yu, Q., Shi, X., Yang, D. and Roth, K.: Effects of stratified active layers on high-
1019   altitude permafrost warming: A case study on the Qinghai-Tibet Plateau, Cryosphere, 10(4),
1020   1591–1603, doi:10.5194/tc-10-1591-2016, 2016.

1021   Pan, X., Yu, Q., You, Y., Chun, K. P., Shi, X. and Li, Y.: Contribution of supra-permafrost

1022 discharge to thermokarst lake water balances on the northeastern Qinghai-Tibet Plateau, J.
1023 Hydrol., 555(November), 621–630, doi:10.1016/j.jhydrol.2017.10.046, 2017.

1024 Pan, Z., Sun, Z., Hu, Y., Chang, Q., Ge, M., Wang, S., Bu, J., Long, X., Pan, Y. and Zhao, L.:
1025 Datasets for research on groundwater flow and its interactions with surface water in an
1026 alpine catchment on the northeastern Tibetan Plateau, China, , (September), 2021.

1027 Pianosi, F. and Wagener, T.: Understanding the time-varying importance of different
1028 uncertainty sources in hydrological modelling using global sensitivity analysis, Hydrol.
1029 Process., 30(22), 3991–4003, doi:10.1002/hyp.10968, 2016.

1030 Ran, Y., Li, X., Cheng, G., Nan, Z., Che, J., Sheng, Y., Wu, Q., Jin, H., Luo, D., Tang, Z. and Wu,
1031 X.: Mapping the permafrost stability on the Tibetan Plateau for 2005–2015, Sci. China Earth
1032 Sci., 64(1), 62–79, doi:10.1007/s11430-020-9685-3, 2021.

1033 Ran, Y. Li, X., Cheng, G., Che, J., Aalto, J. Karjalainen, O. Hjort, J., Luoto, M., Jin, H., Obu, J.,
1034 Hori, M., Yu, Q., Chang, X. (2022) New high-resolution estimates of the permafrost thermal
1035 state and hydrothermal conditions over the Northern Hemisphere. Earth System Science
1036 Data, 14, 865–884. Doi: 10.5194/essd-14-865-2022.

1037 Romanovsky, V.E., and Osterkamp, T.E. (2000) Effects of unfrozen water on heat and mass
1038 transport processes in the active layer and permafrost. Permafrost, and Periglacial
1039 Processes. 11(3), 219-239

1040 Savenije, H.H.G.:HESS Opinions: "The art of hydrology". Hydrol. Earth Syst. Sci., 13, 157–161,
1041 2009

1042 Savenije, H.H.G.: HESS Opinions "Topography driven conceptual modelling (FLEXTopo)".
1043 Hydrol. Earth Syst. Sci. 14 (12), 2681–2692. https://doi.org/10.5194/hess-14-2681-2010,
1044 2010.

1045 Seibert, J. and McDonnell, J. J.: On the dialog between experimentalist and modeler in
1046 catchment hydrology: Use of soft data for multicriteria model calibration, Water Resour.
1047 Res., 38(11), 23-1-23–14, doi:10.1029/2001wr000978, 2002.

1048 Shanley, J. B. and Chalmers, A.: The effect of frozen soil on snowmelt runoff at Sleepers
1049 River, Vermont, Hydrol. Process., 13(12–13), 1843–1857, doi:10.1002/(SICI)1099-
1050 1085(199909)13:12/13<1843::AID-HYP879>3.0.CO;2-G, 1999.

1051 Sheng, Y.: Map of permafrost distribution in the Qilian Mountains. National Tibetan Plateau
1052 Data Center, doi:10.11888/Geocry.tpdc.270456. CSTR: 18406.11.Geocry.tpdc.270456, 2020.

1053 Sivapalan, M., Blöschl, G., Zhang, L. and Vertessy, R.: Downward approach to hydrological
1054 prediction, Hydrol. Process., 17(11), 2101–2111, doi:10.1002/hyp.1425, 2003.

1055 Sjöberg, Y., Frampton, A. and Lyon, S. W.: Using streamflow characteristics to explore
1056 permafrost thawing in northern Swedish catchments, Hydrogeol. J., 21(1), 121–131,
1057 doi:10.1007/s10040-012-0932-5, 2013.

1058 Sokolov, K., Fedorova, L. and Fedorov, M.: Prospecting and evaluation of underground
1059 massive ice by ground-penetrating radar, Geosci., 10(7), 1–14,

1060   doi:10.3390/geosciences10070274, 2020.

1061   Song C, Wang G, Mao T, Dai J, Yang D. 2020. Linkage between permafrost distribution and
1062   river runoff changes across the Arctic and the Tibetan Plateau. Science China Earth Sciences,
1063   63: 292–302

1064   Streletskiy, D. A., Tananaev, N. I., Opel, T., Shiklomanov, N. I., Nyland, K. E., Streletskaya, I. D.,
1065   Tokarev, I. and Shiklomanov, A. I.: Permafrost hydrology in changing climatic conditions:
1066   Seasonal variability of stable isotope composition in rivers in discontinuous permafrost,
1067   Environ. Res. Lett., 10(9), doi:10.1088/1748-9326/10/9/095003, 2015.

1068   Sun, A., Quantified hydrological responses to permafrost degradation in the headwaters of
1069   the Yellow River (HWYR) in High Asia. Science of the Total Environment, 712135632
1070   Permafrost Hydrology Research Domain: Process-Based Adjustment, 2020.

1071   Sun, Z., Zhao, L., Hu, G., Qiao, Y., Du, E., Zou, D., et al: Modeling permafrost changes on the
1072   Qinghai-Tibetan plateau from 1966 to 2100: a case study from two boreholes along the
1073   Qinghai-Tibet engineering corridor. Permafr. Periglac. Process. 31, 156–171,
1074   doi:10.1002/ppp.2022, 2019.

1075   Tananaev, N., Teisserenc, R. and Debolskiy, M.: Permafrost hydrology research domain:
1076   Process-based adjustment, Hydrology, 7(1), doi:10.3390/hydrology7010006, 2020.

1077   Walvoord, M. A. and Kurylyk, B. L.: Hydrologic Impacts of Thawing Permafrost-A Review,
1078   Vadose Zo. J., 15(6), vzj2016.01.0010, doi:10.2136/vzj2016.01.0010, 2016.

1079   Wang, G. X.,Mao, T. X., Chang, J., Song, C. L., and Huang, K. W.: Processes of runoff
1080   generation operating during the spring and autumn seasons in a permafrost catchment on
1081   semi-arid plateaus. J. Hydrol. 550, 307–317. doi:10.1016/j.jhydrol.2017.05.020, 2017.

1082   Wang, L., Koike, T., Yang, K., Jin, R. and Li, H.: Frozen soil parameterization in a distributed
1083   biosphere hydrological model, Hydrol. Earth Syst. Sci., 14(3), 557–571, doi:10.5194/hess-14-
1084   557-2010, 2010.

1085   Wang, P., Huang, Q., Pozdniakov, S. P., Liu, S., Ma, N., Wang, T., Zhang, Y., Yu, J., Xie, J., Fu,
1086   G., Frolova, N. L. and Liu, C.: Potential role of permafrost thaw on increasing Siberian river
1087   discharge, Environ. Res. Lett., 16(3), doi:10.1088/1748-9326/abe326, 2021.

1088   Wang Q F, Jin H J, Zhang T J, et al.: Active layer seasonal freeze-thaw processes and
1089   influencing factors in the alpine permafrost regions in the upper reaches of the Heihe River
1090   in Qilian Mountains (in Chinese). Chin Sci Bull, 61: 2742–2756, doi: 10.1360/N972015-01237,
1091   2016.

1092   Wang, T., Yang, D., Yang, Y., Piao, S., Li, X., Cheng, G. and Fu, B.: Permafrost thawing puts
1093   the frozen carbon at risk over the Tibetan Plateau, Sci. Adv., 6(19), 2–10,
1094   doi:10.1126/sciadv.aaz3513, 2020.

1095   Wang, Y., Yang, H., Gao, B., Wang, T., Qin, Y. and Yang, D.: State Key Laboratory of
1096   Hydroscience and Engineering , Department of Hydraulic School of Water Resources and
1097   Environment , China University of Geosciences , 2018.

1098   Watson, V., Kooi, H. and Bense, V.: Potential controls on cold-season river flow behavior in
1099   subarctic river basins of Siberia, J. Hydrol., 489, 214–226, doi:10.1016/j.jhydrol.2013.03.011,
1100   2013.

1101   Woo, M-K.: Permafrost Hydrology, Springer, 5, 2012.

1102   Wu, T., Li, S., Cheng, G. and Nan, Z.: Using ground-penetrating radar to detect permafrost
1103   degradation in the northern limit of permafrost on the Tibetan Plateau, Cold Reg. Sci.
1104   Technol., 41(3), 211–219, doi:10.1016/j.coldregions.2004.10.006, 2005.

1105   Xiao, Y., Zhao, L., Dai, Y., Li, R., Pang, Q. and Yao, J.: Representing permafrost properties in
1106   CoLM for the Qinghai-Xizang (Tibetan) Plateau, Cold Reg. Sci. Technol., 87, 68–77,
1107   doi:10.1016/j.coldregions.2012.12.004, 2013.

1108   Xie, C., Gough, W.A.: Short Communication: A Simple Thaw-Freeze Algorithm for a Multi-
1109   Layered Soil using the Stefan Equation. Permafrost and Periglac. Process. 24: 252–260, 2013.

1110   Yang, Y., Wu, Q., Jin, H., Wang, Q., Huang, Y., Luo, D., Gao, S. and Jin, X.: Delineating the
1111   hydrological processes and hydraulic connectivities under permafrost degradation on
1112   Northeastern Qinghai-Tibet Plateau, China, J. Hydrol., 569(November 2018), 359–372,
1113   doi:10.1016/j.jhydrol.2018.11.068, 2019.

1114   Ye, B., Yang, D., Zhang, Z. and Kane, D. L.: Variation of hydrological regime with permafrost
1115   coverage over Lena Basin in Siberia, J. Geophys. Res. Atmos., 114(7),
1116   doi:10.1029/2008JD010537, 2009.

1117   Zhang, R., Liu, J., Gao, H. and Mao, G.: Can multi-objective calibration of streamflow
1118   guarantee better hydrological model accuracy?, J. Hydroinformatics, 20(3), 687–698,
1119   doi:10.2166/hydro.2018.131, 2018.

1120   Zhang, T., Frauenfeld, O. W., Serreze, M. C., Etringer, A., Oelke, C., McCreight, J., Barry, R. G.,
1121   Gilichinsky, D., Yang, D., Ye, H., Ling, F. and Chudinova, S.: Spatial and temporal variability in
1122   active layer thickness over the Russian Arctic drainage basin, J. Geophys. Res. D Atmos.,
1123   110(16), 1–14, doi:10.1029/2004JD005642, 2005.

1124   Zhang, X. : High-resolution precipitation data derived from dynamical downscaling using
1125   the WRF model for the Heihe River Basin, northwest China. Theor Appl Climatol, 131:1249–
1126   1259, 2018.

1127   Zhao, L., Zou, D., Hu, G., Du, E., Pang, Q., Xiao, Y., Li, R., Sheng, Y., Wu, X., Sun, Z., Wang, L.,
1128   Wang, C., Ma, L., Zhou, H. and Liu, S.: Changing climate and the permafrost environment on
1129   the Qinghai–Tibet (Xizang) plateau, Permafr. Periglac. Process., 31(3), 396–405,
1130   doi:10.1002/ppp.2056, 2020.

1131   Zhou, J., Kinzelbach, W., Cheng, G., Zhang, W., He, X. and Ye, B.: Monitoring and modeling
1132   the influence of snow pack and organic soil on a permafrost active layer, qinghai-tibetan
1133   plateau of china, Cold Reg. Sci. Technol., 90–91, 38–52,
1134   doi:10.1016/j.coldregions.2013.03.003, 2013.

1135   Zou, D., Zhao, L., Wu, T., Wu, X., Pang, Q. and Wang, Z.: Modeling ground surface

1136 temperature by means of remote sensing data in high-altitude areas: test in the central
1137 Tibetan Plateau with application of moderate-resolution imaging spectroradiometer
1138 Terra/Aqua land surface temperature and ground-based infrared, J. Appl. Remote Sens.,
1139 8(1), 083516, doi:10.1117/1.jrs.8.083516, 2014.

1140

1141 Tables

1142 Table 1. The water balance and constitutive equations used in FLEX-Topo-FS model. In Equation
1143 10, 11, and 12, the S_u and S_{umax} represent root zone reservoirs and their storage capacities in
1144 different landscapes, including vegetation hillslope (S_{umax_V}), alpine desert (S_{umax_D}) and riparian
1145 (S_{umax_R}).

reservoirs	Water balance equations	Constitutive equations
Snow reservoir	$$\frac{dS_w}{dt} = P - M_w \quad (4)$$	$$P_s = \begin{cases} 0; & T > 0 \\ P; & T \le 0 \end{cases} \quad (5)$$ $$M_w = \begin{cases} F_{dd} \cdot T; & T > 0 \\ 0; & T \le 0 \end{cases} \quad (6)$$
Glacier reservoir	$$\frac{dS_g}{dt} = P_l + M_g - Q_g \quad (7)$$	$$M_g = \begin{cases} F_{dd} \cdot T \cdot C_g; & S_w = 0 \text{ and } T > 0 \\ 0; & S_w > 0 \text{ or } T \le 0 \end{cases} \quad (8)$$ $$Q_g = S_g / K_f \quad (9)$$
Root zone reservoir	$$\frac{dS_u}{dt} = P_l + M_w - E_a - R_u \quad (10)$$	$$R_u = (P_l + M_w) \cdot (1 - (1 - \frac{S_u}{S_{umax}})^\beta) \quad (11)$$ $$E_a = E_p \cdot (\frac{S_u}{C_e \cdot S_{u\max}}) \quad (12)$$
Splitter and lag function		$$R_f = R_u D \quad (13); \quad R_s = R_u(1-D) \quad (14)$$ $$R_{fl}(t) = \sum_{i=1}^{T_{lagf}} c_f(i) \cdot R_f(t-i+1) \quad (15)$$

$$c_f(i) = i / \sum_{u=1}^{T_{lagf}} u \quad (16)$$

Fast reservoir $\dfrac{\mathrm{d}S_{\mathrm{f}}}{\mathrm{d}t} = R_{\mathrm{f}} - Q_{\mathrm{f}}$ (17) $Q_f = S_f / K_f$ (18)

1146

1147   Table 2. The parameters of the FLEX-Topo-FS model, and their prior ranges for calibration.

Parameter	Explanation	Prior range for calibration
$F_{dd}(\mathrm{mm}\cdot{}^\circ\mathrm{C}^{-1}\cdot\mathrm{d}^{-1})$	snow degree-day factor	(1-5)
C_g (-)	Glacier degree-factor multiplier	(1-3)
S_{umax_V} (mm)	Root zone storage capacity for vegetation hillslope	(50, 200)
S_{umax_D} (mm)	Root zone storage capacity for alpine desert	(10, 100)
S_{umax_R} (mm)	Root zone storage capacity for riparian	(10, 100)
β (-)	The shape of the storage capacity curve	(0, 1)
C_e (-)	Soil moisture threshold for reduction of evaporation	(0.1, 1)
D (-)	Splitter to fast and slow response reservoirs	0.2
T_{lagF} (days)	Lag time from rainfall to peak flow	(0.8, 3)
K_f (days)	fast recession coefficient	(1, 10)
K_s (days)	baseflow recession coefficient	(10, 100)
k(W/(m·K))	thermal conductivity	2
ω (-)	water content, as a decimal fraction of the dry soil weight	0.12
ρ (kg/m^3)	bulk density of the soil	1000

1148

Figures
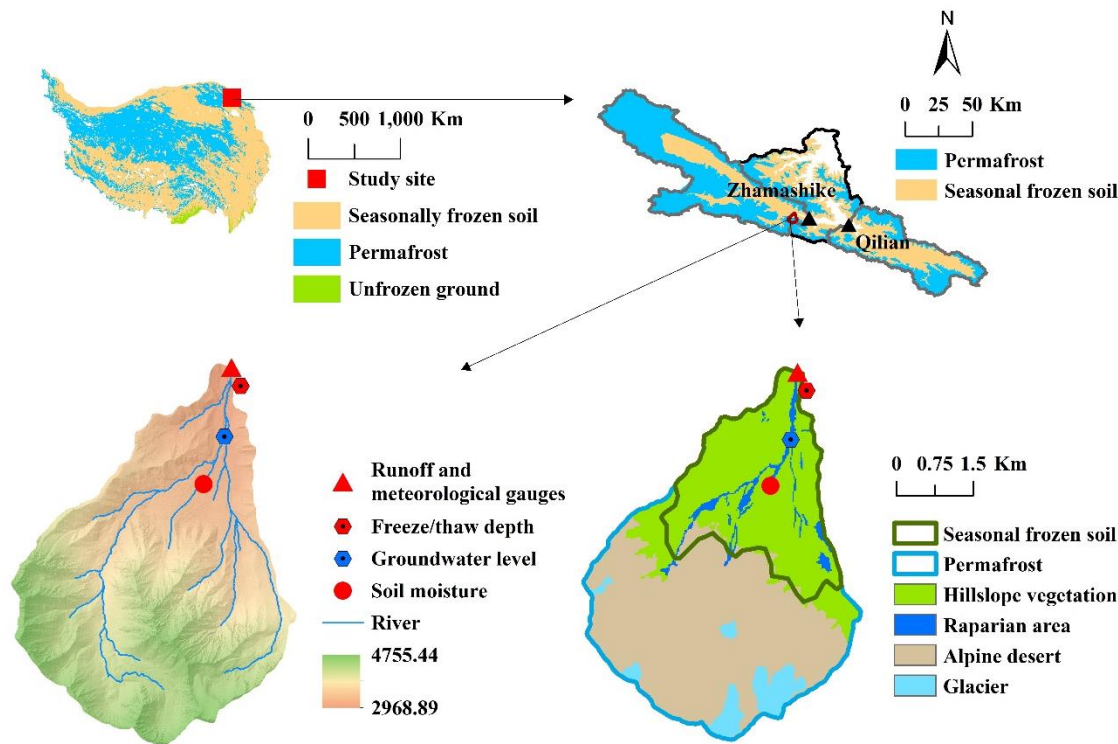
Figure 1. Sketch map of the Qinghai-Tibet Plateau, and the distribution of permafrost and seasonal frozen-soil of the QTP (Zou et al., 2014), and the location of the upper Heihe River basin (up left); sketch map of permafrost and seasonal frozen-soil distribution of the upper Heihe river basin (Sheng, 2020), and the two sub-basins, i.e. Zhamashike and Qilian, and the location of the Hulu catchment (up right); Hulu catchment's digital elevation model (DEM), river channel, runoff and meteorological gauge station (observed from 2011 to 2014), the locations for soil moisture (2011-2013 with data gap), groundwater level (2016-2019), and freeze/thaw depth (bottom left) (2011-2014); landscapes and seasonal frozen-soil / permafrost map of the Hulu catchment (bottom right).

1161
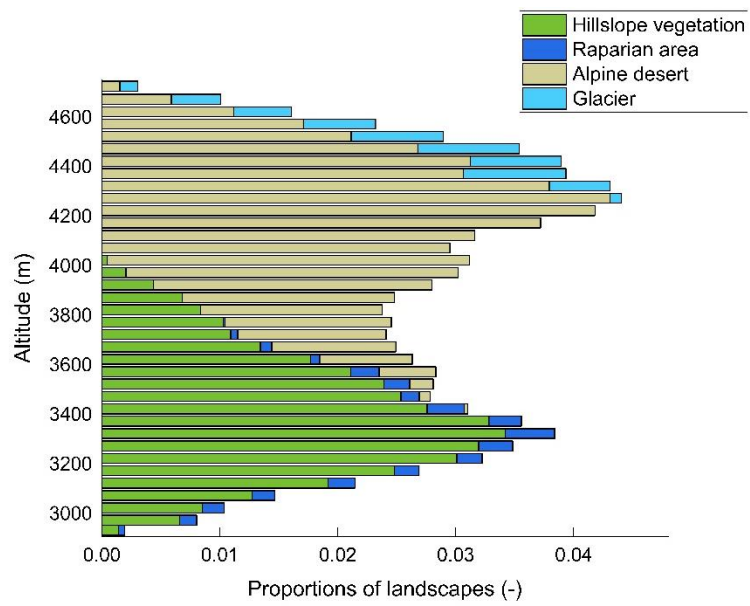
1162   Figure 2. Landscape classification at different elevation bands (with 50m interval) of the Hulu
1163   catchment.

1164
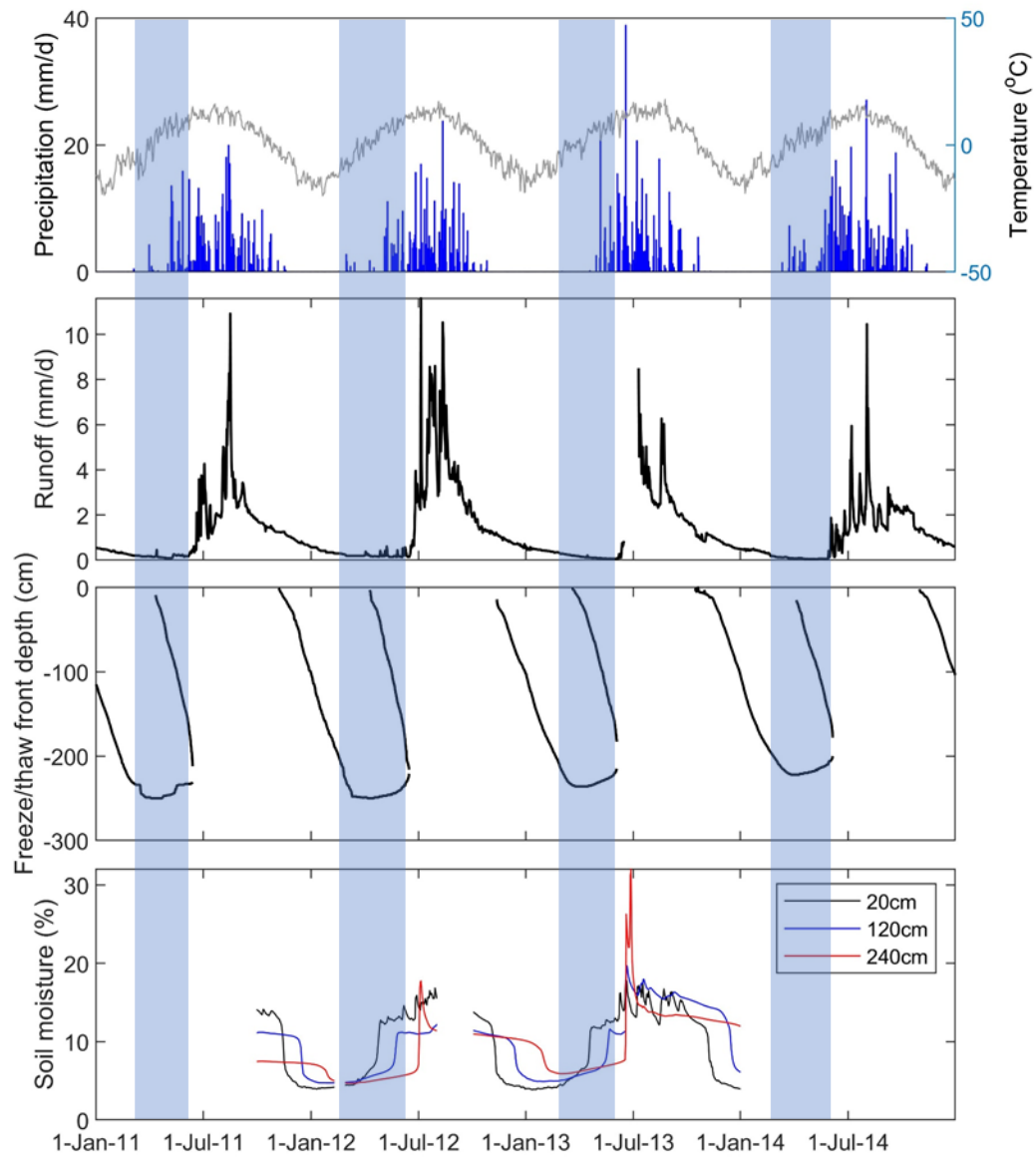
1165 Fig 3. Observed daily precipitation and air temperature; observed daily runoff depth of the
1166 Hulu catchment; observed freeze/thaw front depth; observed soil moisture at the depth of
1167 20cm, 120cm, 240cm.

1168
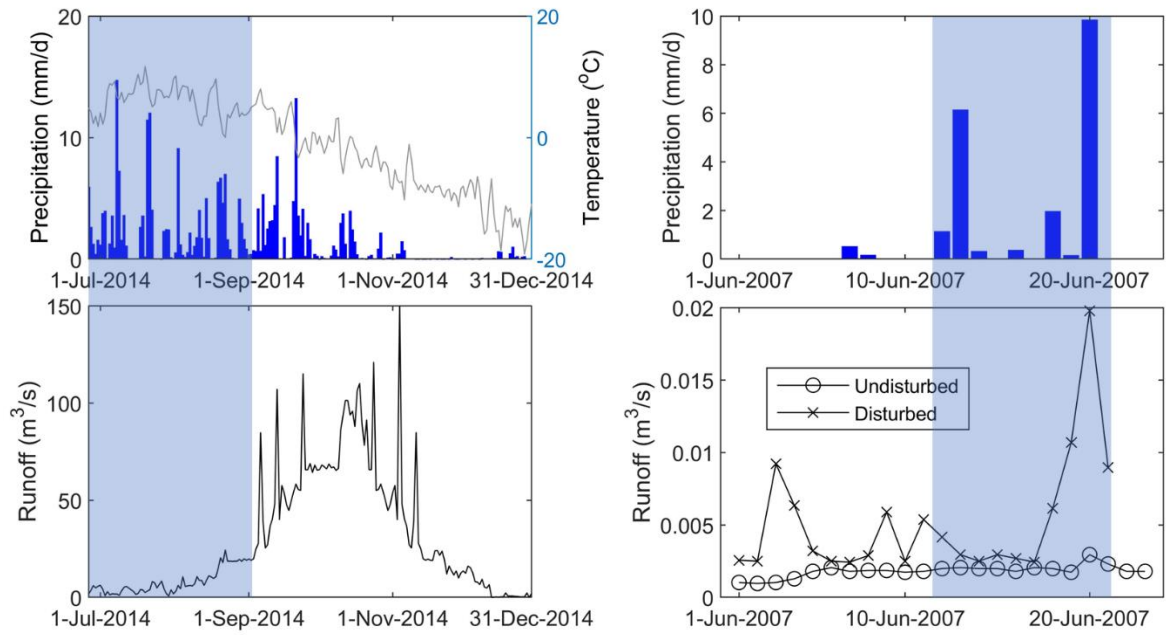
1169   Fig 4. The Little-Runoff in the Early Thawing season (LRET) phenomenon in other places, e.g.

1170   the headwater of Yellow River (Yang et al., 2019), and a small headwater catchment at Cape

1171   Bounty Arctic Watershed Observatory, Melville Island, NU in Canada (Lafrenière and

1172   Lamoureux, 2019)

1173

1174
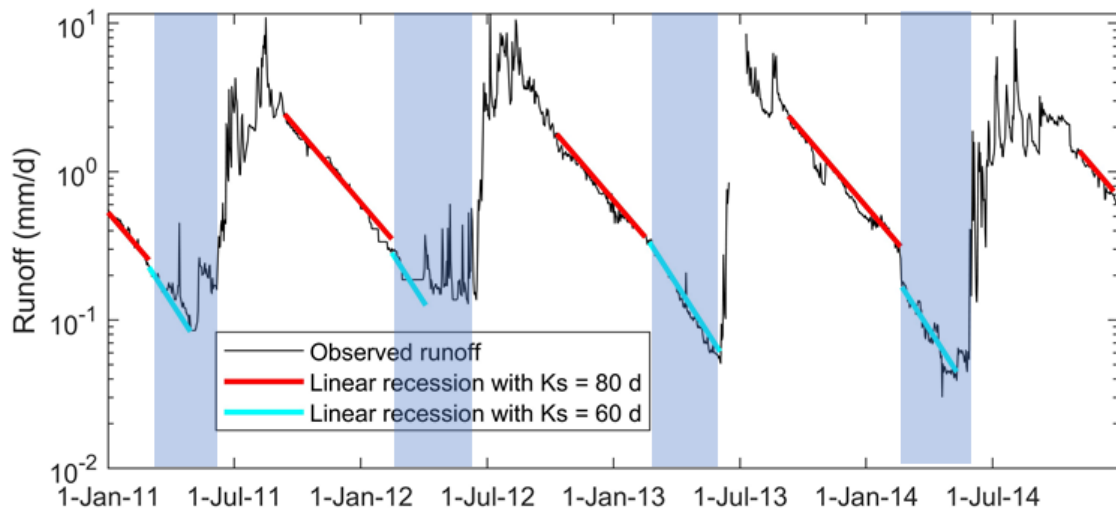
1175   Figure 5. Groundwater recession, from 2011 to 2014, on logarithmic scale, with linear

1176   recession parameter K_s = 80 d in the early recession periods and K_s = 60 d in the end of

1177   recession periods.

1178
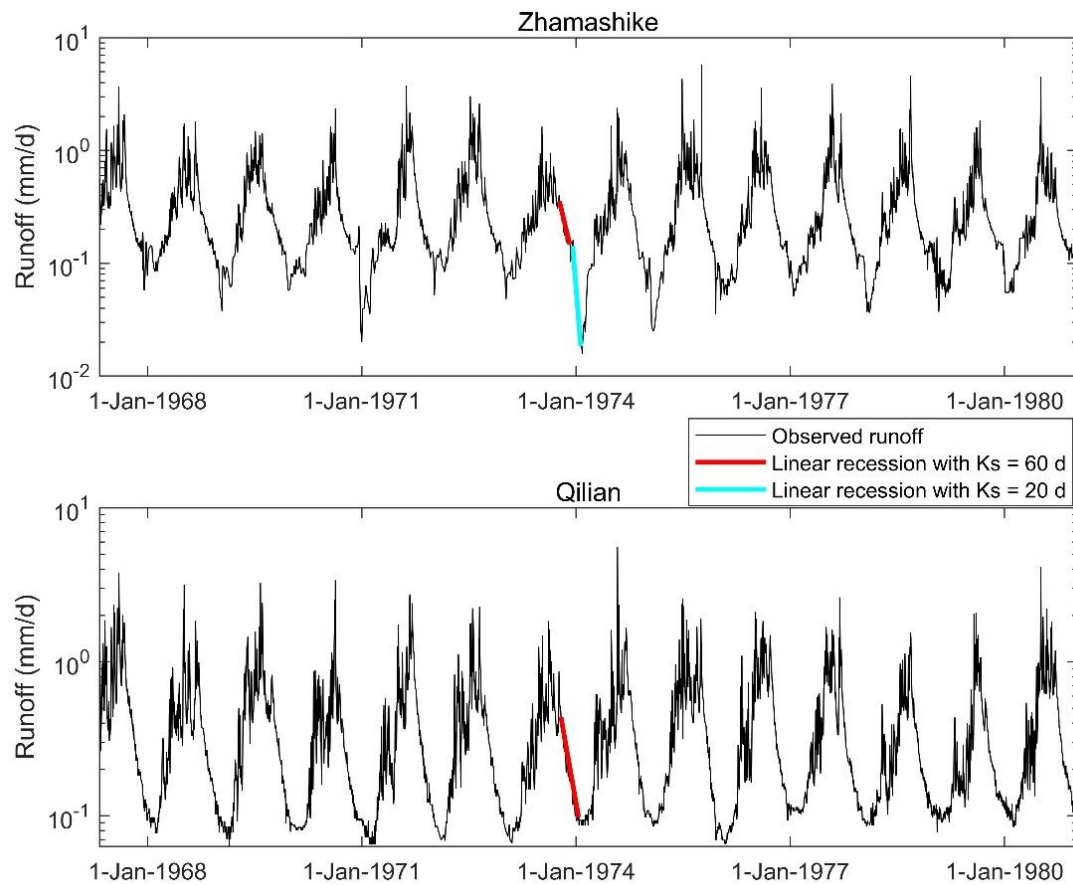
1179   Figure 6. The hydrograph of the Zhamashike and Qilian sub-basin on logarithmic scale, and
1180   the linear recession curve with K_s = 60d and K_s =20d.

1181
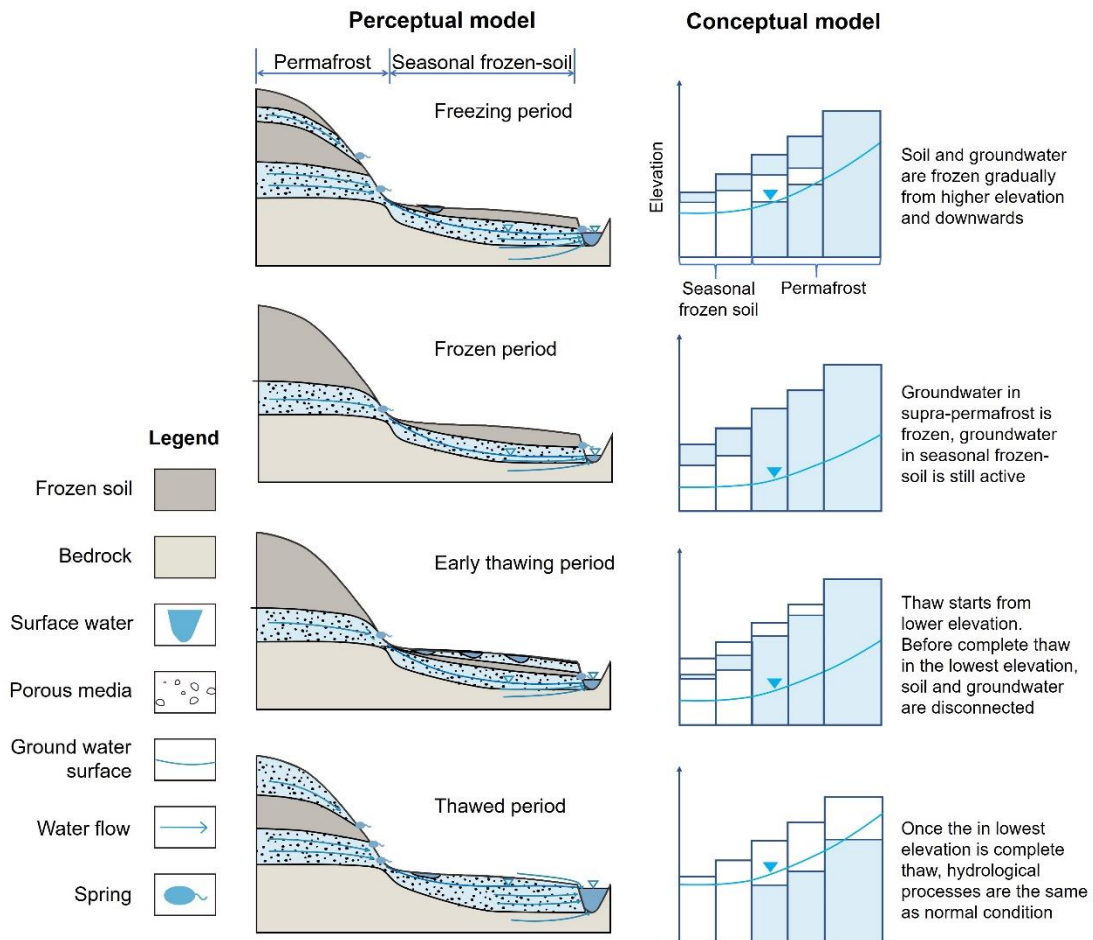
1182   Figure 7 The perceptual and conceptual FLEX-Topo-FS frozen-soil hydrological models.

1183
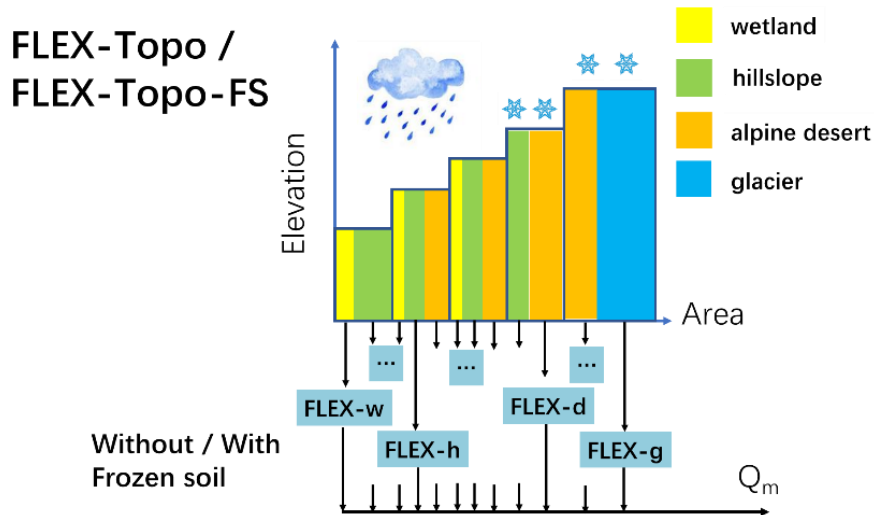
1184   Fig 8. Model structures of FLEX-Topo, and FLEX-Topo-FS. FLEX-w means the module for
1185   wetland, FLEX-h for hillslope, FLEX-d for alpine desert, and FLEX-g for glacier, respectively.

1186

1187
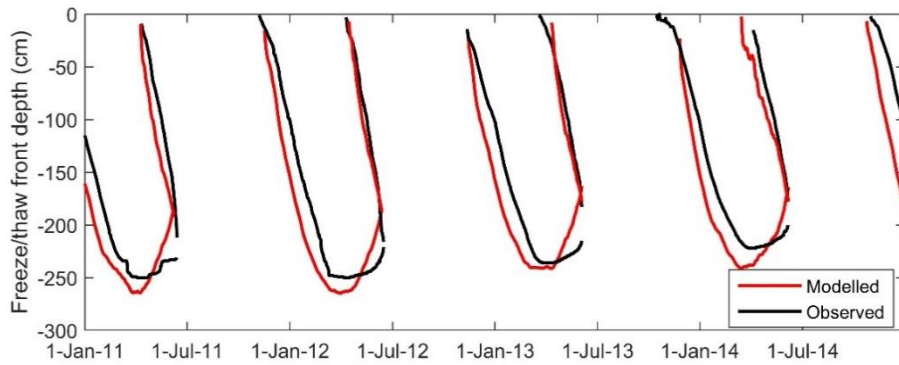
1188   Fig 9. Comparison between simulated freeze/thaw depth by Stefan equation and
1189   observation.

1190

1191
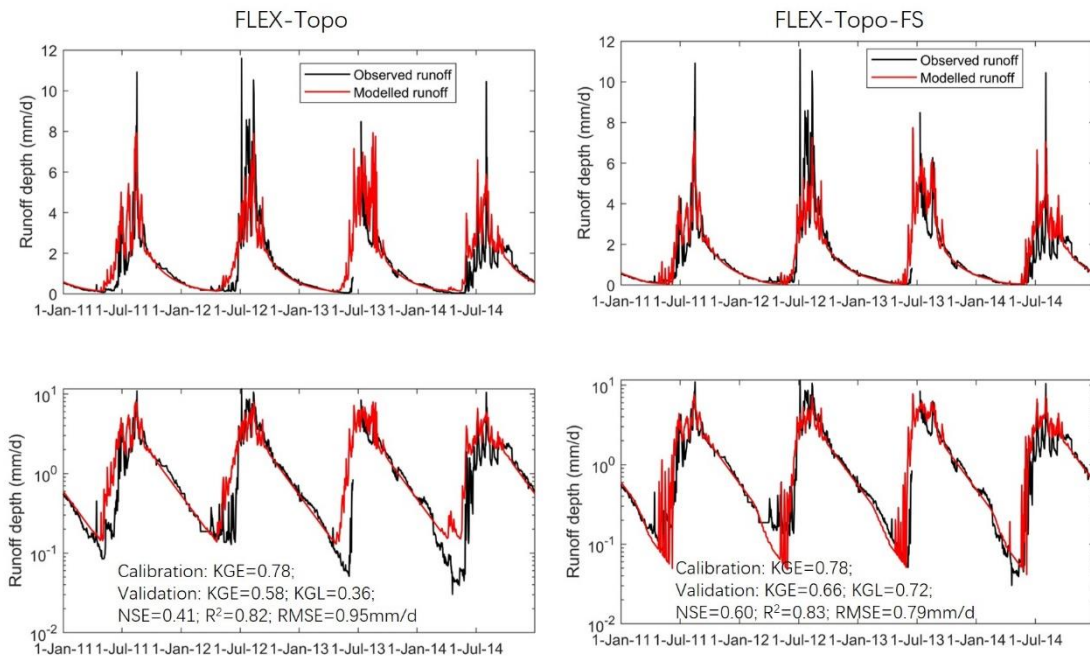
1192   Figure 10. Modeling results of FLEX-Topo and FLEX-Topo-FS models, and the comparisons
1193   with observation, on both normal and logarithm scales.

1194
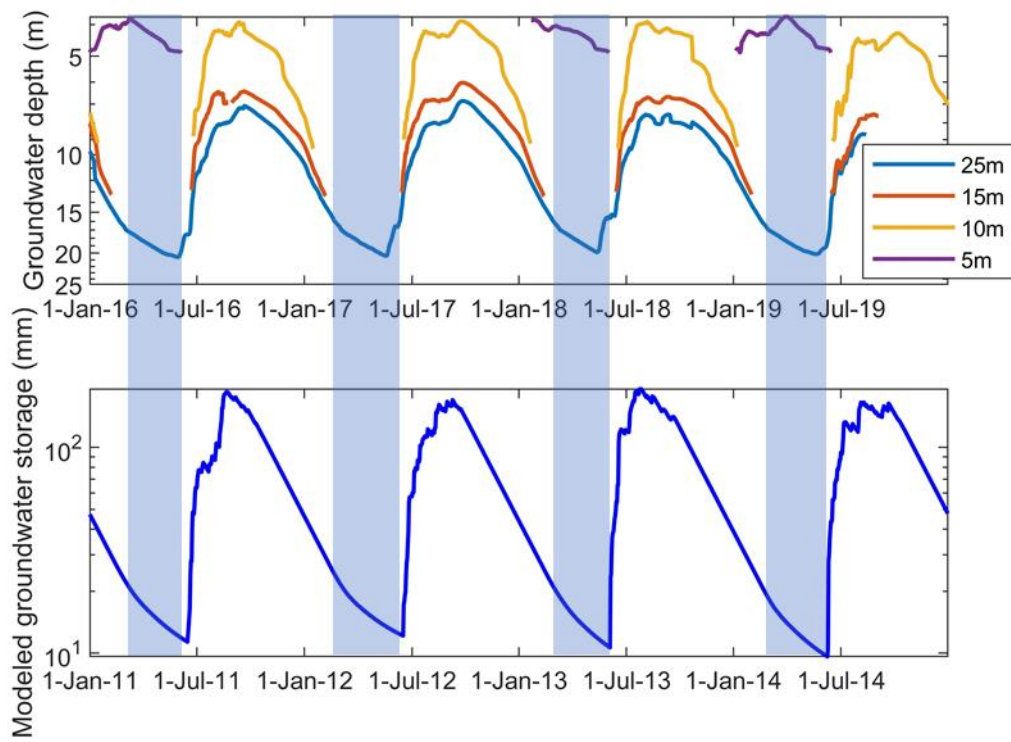
1195 Figure 11. Observed groundwater depth from 2016 to 2019 at WW01 wells at depth of 5m,
1196 10m, 15m, and 25m. And the simulated groundwater storage by the FLEX-Topo-FS model
1197 from 2011 to 2014.
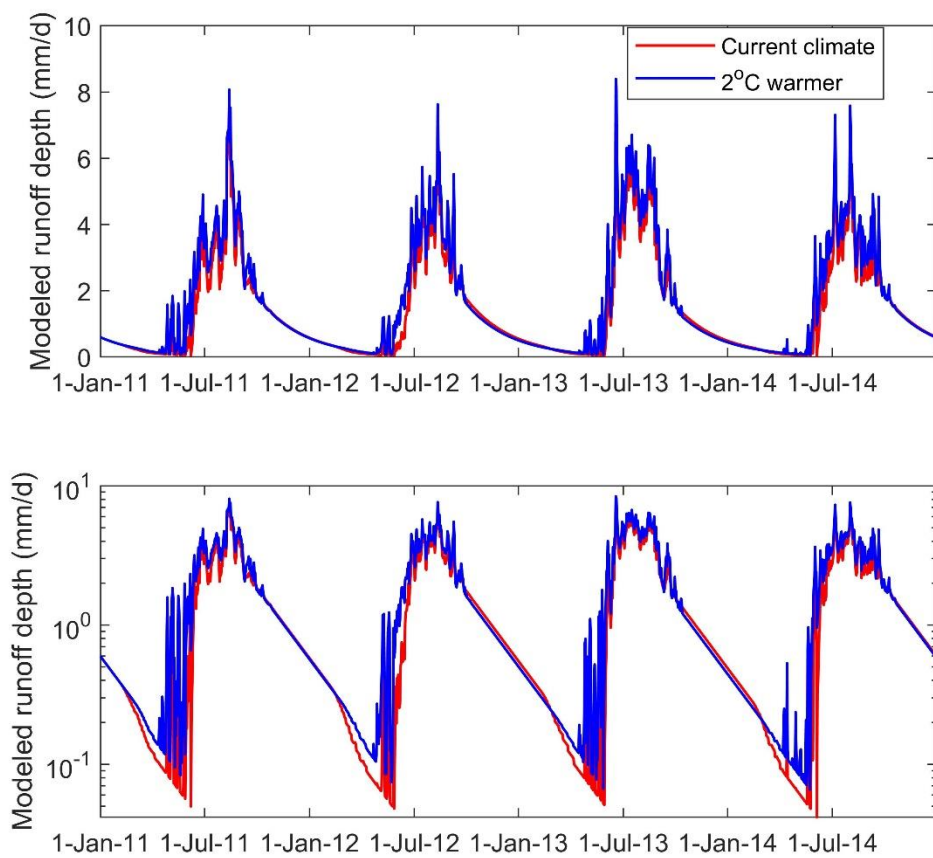
1198

1199 Figure 12. Simulated hydrograph in current climate condition, and the 2°C warmer
1200 condition.